The Development and Characterization of Lightweight $(Ca_{1-x},Mg_x)Zr_4(PO_4)_6$ Ceramics

by

Dean-Mo Liu

Thesis submited to the Faculty of the

Virginia Polytechnic Institute and State University

in partial fulfillment of the requirements for the degree of

Master of Science

in

Materials Engineering

APPROVED:

Dr. Jesse J. Brown Jr., Chairman

Dr. Ronald S. Gordon, Department Head

Dr. Ronald G. Kander

May 1991

Blacksburg, Virginia

The Development and Characterization of

Lightweight $(Ca_{1-x},Mg_x)Zr_4(PO_4)_6$ Ceramics

by

Dean-Mo Liu

Jesse J. Brown, Jr., Chairman

Materials Engineering

(ABSTRACT)

Lightweight $(Ca,Mg)Zr_4(PO_4)_6$ (CMZP) ceramics have been fabricated with relative densities ($\rho_{lightweight}/\rho_{dense}$) of less than 0.35 by the polymer foam technique, and higher than 0.35 by the polymer powder technique. The polymer powder method forms an inhomogeneous pore structure having average pore sizes of 30-80 μm compared with the polymer foam method, which yields a large and uniform pore structures with pores 250-300 μm in diameter.

The thermal expansion of the lightweight CMZP ceramics varies from positive ($+2.7x10^{-6}/°C$) to negative ($-2.6x10^{-6}/°C$) with increasing grain size. The lightweight CMZP ceramics exhibit an excellent thermal shock resistance and this resistance is improved by increasing porosity.

Mechanical properties including tensile strength, compressive strength, Modulus of rupture (MOR), and Young's moduli have been determined and vary exponentially with porosity. The strengths of the lightweight CMZP ceramics are superior to those of lightweight ZrO_2 with the same bulk density. Young's

moduli, which were determined using a sonic velocity technique, range from about 5 GPa to 30 GPa, depending on the composition and the relative density. Furthermore, corrosion studies show that lightweight CMZP ceramics possess high resistance to acid corrosion at ambient temperature.

ACKNOWLEDGEMENTS

The author wishes to express his gratitude for the help and guidance given by his advisor, Dr. J.J. Brown, Jr.. In addition, he wishes to express his thanks to three special persons, Dr. Tawai Sun and Dr. Tingkai Li, for their useful discussion and Dr. D.A. Hirshfeld for her editorial assistance.

He also wishes to express his thanks to Dr. Ronald S. Gordon and Dr. Ronald G. Kander for serving on his committee.

TABLE OF CONTENTS

LIST OF FIGURES

CHAPTER 1. INTRODUCTION

The rising costs of petroleum products and other energy sources have brought attention to the importance of energy utilization, particularly energy savings and service efficiency. One method to improve energy utilization is to develop new materials having characteristics such as low thermal conductivity to reduce heat dissipation during operation, low coefficient of thermal expansion to minimize thermal-shock-induced fracture when subjected to cyclic thermal environments, and good thermal stability for high-temperature applications. Currently, lightweight ceramics are widely used as thermal insulation and filter systems: the thermal protection system of the space shuttle and the filtration systems for molten metals and hot gas clean up. These applications of lightweight ceramics require high thermal shock resistance, low thermal conductivity, and sufficient mechanical strength. In addition, the processing techniques used to fabricate lightweight ceramics determine the structure which has a significant influence on their performance.

The development of a lightweight ceramic having both a low coefficient of thermal expansion and a low thermal conductivity has been initiated by exploring a new class of ceramic materials known as [NZP], i.e., $NaZr_2(PO_4)_3$, which has these desired properties[1,2,3]. The Na^{1+} ions in the [NZP] structure allow a richness of ionic substitution without changing the crystal structure. One

substance, $(Ca_{1-x},Mg_x)Zr_4(PO_4)_6$ (CMZP) where x lies between 0.0 and 0.5, possesses an ultra-low coefficient of thermal expansion (CTE), high thermal shock resistance, and a thermal conductivity which is lower than that of conventional thermal barriers. Therefore, it appears to be a strong candidate for thermal barrier applications and structural components in heat engine applications. Being a phosphate material, it is also a candidate for biotechnology applications such as supports of biological catalysts[4].

The goal of this research is to develop processing techniques and to characterize the properties of lightweight $(Ca,Mg)Zr_4(PO_4)_6$ ceramics. Properties including thermal expansion, corrosion resistance, and thermal-shock resistance of lightweight CMZP ceramics were investigated. In order to make lightweight CMZP ceramics viable in structural applications, the microstructure and related mechanical properties such as strength and elastic moduli were also studied. Furthermore, the thermal conductivity of dense CMZP was determined.

CHAPTER 2. LITERATURE REVIEW

2.1 Processing of Porous Ceramics

Lightweight ceramics may have four basic structures: (1) tangle fiber networks, e.g., the thermal protection system of the space shuttle formed by sintering silica glass fibers with a high temperature binder; (2) particulate networks, e.g., porous glass-ceramics formed using sol-gel methods; (3) open-cell structures, e.g., filters produced by coating open-cell polymer foams with a ceramic; and (4) closed-cell structures, e.g., sintered hollow spheres.

Open-cell ceramics, which are fabricated by coating reticulated polymer substrates with a ceramic slurry, possess a variety of unique properties; such as controllable pore size, controllable tortuosity, and complex ceramic shape for different applications, and are favorable for many applications as pointed out by Lange et al[5].

Closed-cell glasses are formed by sintering hollow glass spheres. Green[6] found that the densification behavior of the glass spheres was complex involving uniform shrinkage of the spheres, local densification, deformation of the sphere, and coarsening of the cells.

Fujiu et al[7] fabricated porous silica having closed-cell structures by controlling gel viscosity and foaming agent concentration in a sol-gel method, but

the porous silica densified as the temperature increased above 1000°C, indicating that this fabrication technique is inappropriate for high-temperature applications.

In the present research, the method used to fabricate porous ceramics with primarily a closed-pore structure is to mix polymer and ceramic powders, leaving voids or pores after sintering.

2.2 Permeability of Porous Ceramics

The permeability of lightweight ceramics is certainly dependent on the pore structure. Wiggs[8] examined the effects of pores of various degrees of complexity on permeability and found that there is no effect on permeability for closed pores or pores with only one entrance, but the permeability is affected if the pores have several constricted entrances or have other larger internal constrictions.

2.3 Thermal Expansion Behavior

$(Ca_{1-x},Mg_x)Zr_4(PO_4)_6$ (CMZP), which has an ultra-low thermal expansion can be synthesized using solid-state reaction and sol-gel methods.

The thermal expansion of [NZP] is explained in terms of a structural model based on rotation of the polyhedral network of the lattice[9,10]. The crystal structure of [NZP] is a hexagonal structure with $R\bar{3}C$ space symmetry, as schematically shown in Fig. 2.1[10], and is built up of PO_4 tetrahedra and ZrO_6 octahedra which are linked by corners to form a three-dimensional network. The bonds are strong and the skeletons are stable. These bonds can bend and result in a small rotation without breaking the structure. The interstitial sites M' and M'' which are the holes or vacancies in the strong skeleton can be left vacant without changing the crystal structure and allow a variety of ionic substitutions[11,12]. For example, Ca ions are substituted by Mg ions in CMZP crystal structure.

The framework structure of [NZP], Fig. 2.1, expands in the **c**-axis direction on heating while the PO_4 groups rotate, in the meantime the structure contracts in the **a**-axis direction[10]. In contrast, the PO_4 groups can rotate in the opposite direction which result in an expansion in the **a**-axis direction and thus the structure contracts in the **c**-axis direction. In general, the displacements in the structure result in thermal expansion anisotropy (TEA) and exhibit a near-zero bulk coefficient of thermal expansion (CTE) as described by the following equation[1]

$$\alpha_{bulk} = \frac{2\alpha_a + \alpha_c}{3} \qquad (2\text{-}1)$$

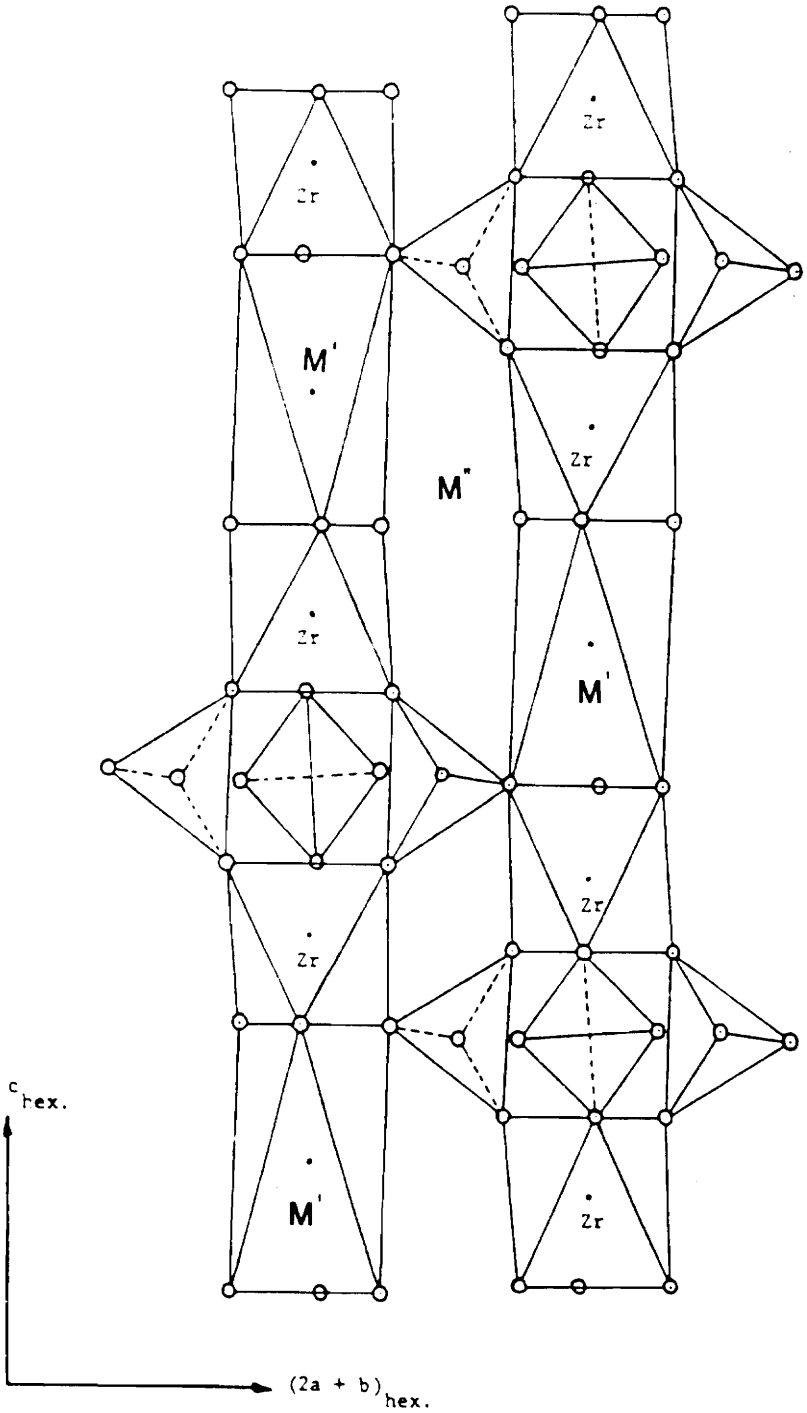

Figure 2.1 Schematic drawing of [NZP] structure. (after Lenain et al, 1987)

where α_a = average CTE in the **a**-axis direction

α_c = average CTE in the **c**-axis direction

2.4 Thermal Expansion Hysteresis

Thermal expansion hysteresis, in which the expansion curve upon heating is substantially different from that upon cooling, is caused by the presence of internal microcracks which result from TEA during processing[13].

Rice et al[14] and Cleveland et al[15] observed that the microcracks are dependent on the grain size. No microcracks occur in small-grained solids because the residual stresses resulting from TEA are not sufficient to nucleate microcracks, thus no thermal expansion hysteresis is observed. On the other hand, in large-grained solids, residual stresses cause microcracks resulting in large thermal expansion hysteresis.

2.5 Thermal Conductivity

The conduction process for heat-transfer in ceramic materials is primarily controlled by the transmission of phonons and photons, the former has a greater amount of energy, while the latter has a lesser amount of energy. In general, phonon conduction dominates the heat conduction process[16].

The fundamental equation of thermal conductivity is:

$$q = -k A \left(\frac{dT}{dx}\right) \qquad (2\text{-}2)$$

where q = amount of heat flowing per unit time through an area A

dT/dx = temperature gradient in a direction perpendicular to A

k = thermal conductivity

The effect of composition on thermal conductivity can be explained by the Debye equation which is based on the concept of a solid as a system of coupled oscillators which transmit thermoelastic waves[16]. For different compositions, the thermoelastic waves are affected because the mean free path and the velocity of the waves are different. The Debye equation is:

$$k = 1/4\ \rho\ c\ v\ \lambda \qquad (2\text{-}3)$$

where ρ = Bulk density (g/cm^3)

c = Speed of light (cm/sec)

λ = Mean free path of the wave (cm)

v = Average velocity of the wave (cm/sec)

It is apparent that any factors which decrease the mean free path of the thermoelastic waves will reduce the thermal conductivity. The major factor affecting the mean free path is the symmetry and order of the crystalline lattice.

Materials having a simple cubic lattice are expected to give rise to fewer anharmonic vibrations and to have a higher thermal conductivity than complex crystalline lattices[16], such as CMZP.

Two other factors affecting the thermal conductivity are pores and microcracks. Loeb[17] and Francl et al[18] investigated porosity-related thermal conductivity and obtained this relation for porous materials:

$$k_p = k_s (1-p) \qquad (2\text{-}4)$$

where k_s = Thermal conductivity of dense material

k_p = Thermal conductivity of porous material

p = porosity which equals $1-(\rho/\rho_s)$, ρ is bulk density and ρ_s is theoretical density.

Equation (2-4) indicates that the thermal conductivity is decreased with increasing porosity. This is because pores act as a scattering center for the phonon, reducing the mean free path of the phonon. The effects of microcracks on thermal conductivity were investigated by Hasselman[19] and Siebeneck et al[20]. They found that the thermal conductivity is decreased with increasing temperature in fine-grained materials (1 μm) and further decreased in large-grained materials having extensive microcracking.

2.6 Thermal Shock Resistance

The resistance of brittle ceramic materials to failure as a result of thermal stress conditions, especially resulting from a rapid change in temperature difference, is extremely important.

The concepts of thermal stress fracture of brittle materials indicate that the resistance of thermal stress or shock damage increases with high values of tensile strength and thermal conductivity, and low values of CTE, Young's modulus, Poisson's ratio, and emissivity. Besides these factors, Becher et al[21] found that the thermal shock resistance of a material is increased as the dimensions of the material are decreased. For porous materials, the thermal stress resistance is also affected by the porosity dependence of fracture strength and Young's modulus[22]. Thus, the resistance to thermal shock of ceramic materials can be presented as[23]

$$\Delta T = \frac{S_t(1-\nu)}{E\,\alpha}\left(\frac{k}{0.31 r_m h}\right) \qquad (2\text{-}5)$$

where S_t = Tensile strength (psi)

α = Coefficient of thermal expansion (/°C)

ν = Poisson's ratio

E = Young's modulus (GPa)

r_m = Half thickness of sample (cm)

h = Surface heat transfer coefficient (cal/sec/cm^2/°C)

Hasselman[24,25] proposed that crack propagation under thermal stress conditions generally occurs in the absence of external forces. The driving force for crack propagation rises from the stress field due to thermal expansion anisotropic (TEA) within the thermally shocked materials. Microcracked materials usually exhibit high thermal shock resistance which is attributed to lower values of Young's moduli[24].

The influence of grain size on thermal shock resistance was investigated by Gupta[26] for Al_2O_3. He found that thermal stress resistance is increased with increasing grain size because the propagation of cracks already formed are decreased. This is consistent with the concept of "effective crack length" proposed by Hasselman[24], who stated that cracks propagate in a quasi-static manner in a finite temperature change; thus reduce the thermal-stress-induced fracture.

2.7 Mechanical Properties

Mechanical behavior, especially strength and elastic modulus, of lightweight ceramics generally exhibit a complex dependence on the microstructure. Usually, the properties of the lightweight ceramics are closely related to the average rather than the extremes of the microstructural characteristics[27]. However, strengths

often depend critically on microstructural extremes rather than average. Porosity is probably the most important factor that affects strength and elastic behavior.

2.7.1 Elastic Modulus

Elastic modulus is primarily dependent on porosity. Rice[27] pointed out that the major factors affecting the elastic modulus are the inhomogeneous distribution of pores and variations in pore shape and size. The change in elastic modulus for packed particle arrays has been considered by Rice[27] and Spriggs[28]. The models of Rice and Spriggs are based on the assumption that the elastic modulus can be related to the cross-sectional area of the neck region between particles and that axial extension is the primary form of deformation.

As pointed out by Agarwal et al[29], various theories have been developed for materials consisting of a continuous matrix and a dispersed second phase of specific shape and orientation, however, they do not apply to porous materials with interconnected pores. Recently, Gibson et al[30] developed an equation based on micromechanical models for open-cell solids having bulk density less than 30% of theoretical density and indicated that the elastic modulus is related to the relative density (ρ/ρ_s) of the solids by:

$$\frac{E}{E_o} = C \left(\frac{\rho}{\rho_s}\right)^n \qquad (2\text{-}6)$$

where E = Young's modulus of the porous material

E_o = Young's modulus of dense material

C = Constant

For open-cell solids, where n=2, C=1.0, eq.(2-6) produces a good description for elastic behavior. More recently, Nielsen[31] developed a model to describe Young's modulus-porosity relation using a shape factor, ϕ:

$$\frac{E}{E_o} = \frac{(1-p)^2}{1+(1/\phi-1)\,p} \qquad (2\text{-}7)$$

This equation generally applicable to all ranges of porosity. A shape factor, ϕ, less than 0.4 indicates a continuous pore phase is present in the solid, while a shape factor higher than 0.6 represents a discontinuous pore phase. When the shape factor lies between 0.3 and 0.7, the pore phase resembles ribbons.

For porous materials, the elastic modulus can be expressed empirically by an exponential dependence, e^{-bp}, which is a widely used relation[28].

$$E = E_o\, e^{-bp} \qquad (2\text{-}8)$$

where b is a material constant.

2.7.2 Mechanical Strength

The relationship between strength and porosity has been extensively studied during the last two decades[32]. The most widely used relation for mechanical strength as it is for the elastic modulus is the exponential relation which was first proposed by Ryshkewitch[33]:

$$S = S_o e^{-bp} \tag{2-9}$$

where S is the strength of the porous material, S_o is the zero-porosity strength, and b is determined by the complexity of the pore structure.

Schiller[34] developed a relation which assumed that the stress around a spherical pore is a function of the stress in the absence of pores and the ratio of the average pore radius to the average pore spacing:

$$\sigma = \sigma_o f(r/s) \tag{2-10}$$

where σ_o = Stress in the absence of any pores

r = Average pore radius

s = Center distance between pores

Schiller found that a critical volume fraction porosity of less than one is required for a body to have strength, as illustrated in Fig. 2.2. Hrma et al[35] developed

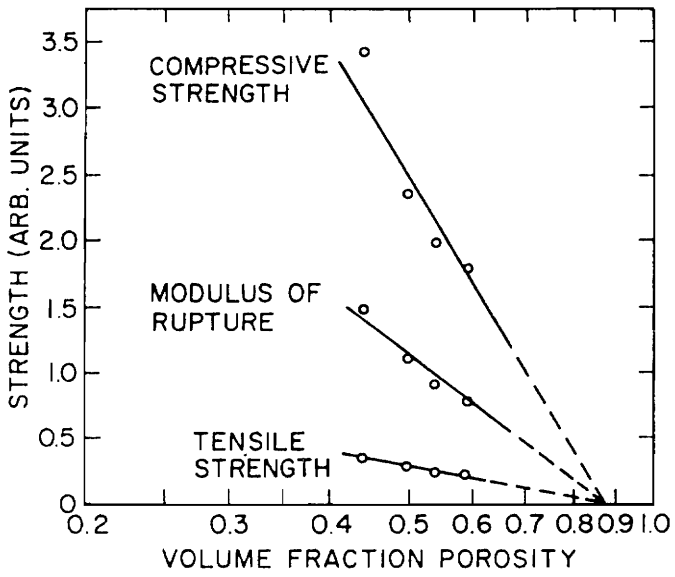

Figure 2.2 Strength versus porosity for plaster (after Schiller,1958).

a body built up of spherical particles in a similar fashion to Schiller's model. Hrma et al obtained a similar result as that proposed by Schiller and concluded that there must be a sufficient number of solid particles connected to provide strength.

Spriggs[28] used the exponential relation to account for open porosity (p_1) and closed porosity (p_2):

$$S = S_o \exp(-b_1 p_1 + b_2 p_2) \qquad (2\text{-}11)$$

where b_1 and b_2 are material constants. Equation (2-11) does improve the strength-porosity correlation, but it exhibits less accuracy for predicting the strength for a material with closed pores because the pores can be at grain boundaries or within grains. Moreover, both experimental and theoretical evidence has shown that the location of the pores has a greater effect on strength than whether the pores are open or closed[32].

Recently, Gibson et al[30] pointed out that at high porosity the fracture mode of cellular solids is controlled by cell-edge bending and/or cell-wall stretching when the solids are subjected to a compressive stress. This concept is consistent with the experimental observation of Ryshkewitch in porous ZrO_2 and Al_2O_3[33]. Here, the test specimens were less brittle with increasing porosity and failure occurred both in tension and shear but never in true compression.

As for the porosity dependence of the material constant b in the relation e^{-bp}, Gannon[36] indicated that it usually is larger due to inhomogeneous pore distribution and variety of pore shapes, but is smaller for materials possessing uniform pore shape and uniform pore distribution. Kundsen[37] proposed a set of models to describe the relationship between strength and porosity based on the different packing arrangements of coalescing spheres. Kundsen found that cubic packing has the smallest b value, orthorhombic has an intermediate b value, and rhombohedral has the highest b value. This indicates that the more complex the pore shape, the higher the porosity dependence.

CHAPTER 3.EXPERIMENTAL PROCEDURE

3.1 CMZP Powder Preparation

3.1.1 Solid-State Reaction

Single phase CMZP powders were synthesized using stoichiometric amounts of $CaCO_3$, $MgCO_3$, ZrO_2 and $NH_4H_2PO_4$. The mixture was homogenized in acetone either by hand mixing in a mortar with a pestle or by ball milling and then air dried. The dry powder was calcined at different temperatures to drive off the volatiles: 200-250°C for 16-20h, 600-650°C for 4-8h and 1000-1280°C for 24-72h. Before each heat treatment the material was thoroughly ground to ensure material homogeneity. The resultant powders were ground by ball milling to particle sizes of 3-5 μm and then characterized by X-ray diffraction.

3.1.2 Sol-Gel Synthesis

In sol-gel processing, the starting raw materials $Ca(NO_3)_2 \cdot 4H_2O$, $Mg(NO_3)_2 \cdot 6H_2O$, $ZrO(NO_3)_2 \cdot xH_2O$ and $NH_4H_2PO_4$ were prepared to form 1.0M aqueous solutions. The zirconium nitrate and a nitrate solution containing both

Ca and Mg nitrates with the desired molar ratios were mixed first. The phosphate solution was then added slowly to the nitrate solution, which was stirred vigorously. The pH value of the solution was kept at 7 by adding ammonium hydroxide until the solution became a gel. The gel was dried at 60-80°C for 16h, and then calcined at 600-700°C for 16-20h to decompose the nitrates and resulted in fine single phase powders having a particle size of 45 nm.

3.2 Preparation of Lightweight CMZP Ceramics

3.2.1 Polymer Foam Method

Reticulated polyurethane foam (a flexible porous cellular plastic) with a pore size of 100 ppi (100 pores per inch, which is equivalent to a pore size of 250-300 μm) was used. The foam was impregnated with a ceramic slurry consisting of deionized water, 10-25 w/o of CMZP powders, 5-25 w/o of cellulose ether binder (based on the weight of the CMZP powders), and 0-5 w/o ZnO as a sintering aid. The slurry-coated foam was heat-treated at 1200-1300°C for 0.2-24h with a heating rate of 100°C/h. The relative density of lightweight CMZP ceramics made by this method usually is less than 0.35.

3.2.2 Polymer Powder Method

The CMZP powders were mixed with 5-22.5 w/o of poly(vinyl chloride) having particle sizes of 20-30 μm and 0-5 w/o ZnO. The mixture was pressed to form a 12.7 mm x 12.7 mm x 100 mm rectangular bar at a hydraulic pressure of 140 MPa. The bar was heated using the same firing conditions as those in the polymer foam method. Lightweight CMZP ceramics having relative densities from 0.35 to 0.85 were formed.

3.3 Preparation of Lightweight ZrO_2

For comparison, lightweight ZrO_2, which is a conventional thermal barrier material, was made using the polymer powder method described above. Zirconia, 5-25 w/o of poly(vinyl chloride), and 4.2 w/o of MgO were mixed, pressed into bars, then heat-treated at 1500°C for 6h with a heating rate of 100°C/h. Lightweight ZrO_2 having relative densities from 0.2 to 0.83 was formed.

3.4 Permeability

The pore structures of the lightweight CMZP ceramics were characterized using scanning electronic microscopy and permeability tests. The apparatus for measuring permeability is illustrated in Fig. 3.1 (ASTM, E128 gas-water permeability). Lightweight CMZP ceramics were prepared in a cylindrical shape with dimensions of 12.7 mm diameter x 25.4 mm length, wrapped with parafilm and sealed by two plastic tubes to ensure that the only open channel is the cross-sectional area of the specimen. The permeability was calculated using the equation[37]:

$$\text{permeability (Darcy)} = \frac{\mu Q L}{A (\Delta p)} \qquad (3.1)$$

where μ = Viscosity of air (centipoise)

L = Length or thickness of specimen (cm)

A = Cross-sectional area of specimen (cm^2)

Q = Air flow rate (cm^3/min)

Δp = Pressure drop (atm)

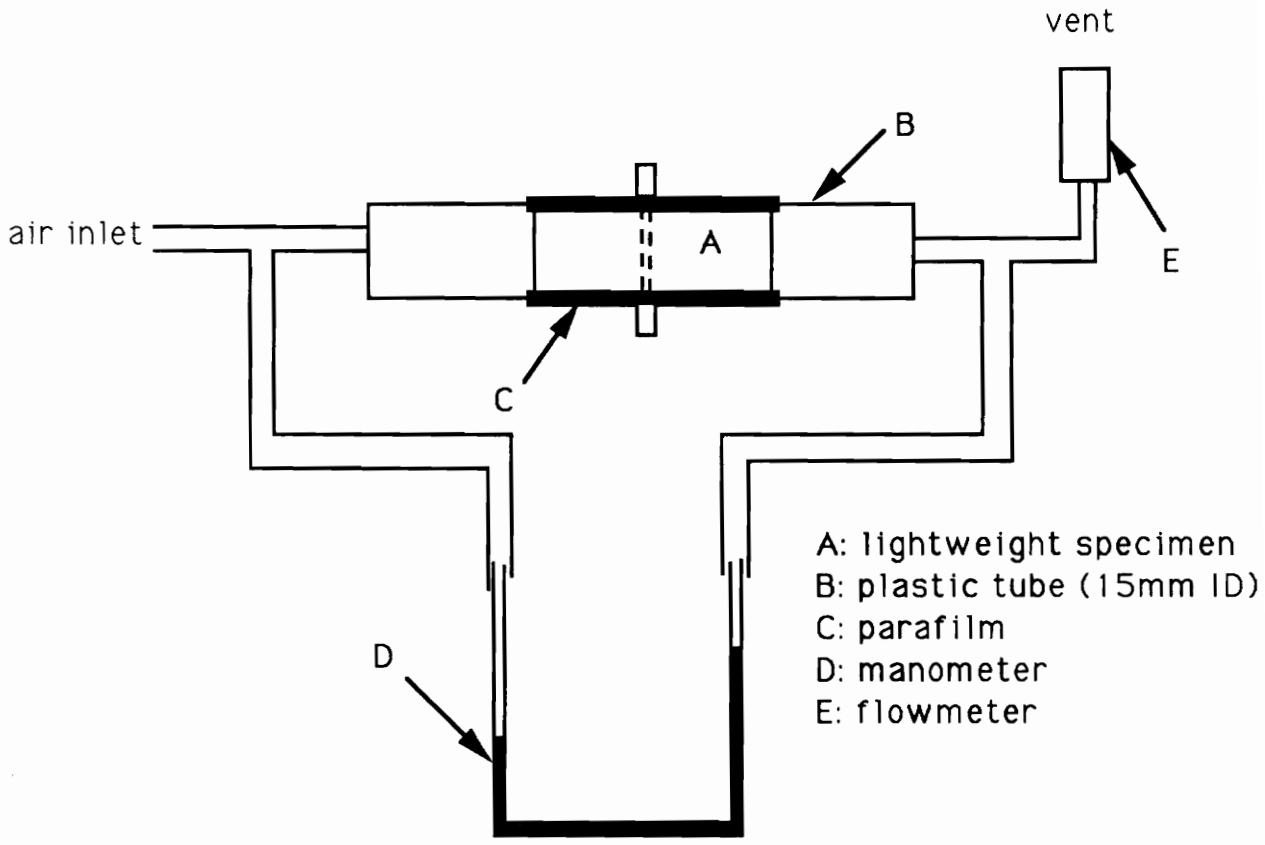

Figure 3.1 Apparatus for permeability measurement

3.5 Thermal Expansion Measurement

Thermal expansion of both dense and lightweight CMZP ceramics was determined using a Netzsch differential dilatometer (Model 402 ED) with a heating rate of 10°C/min from ambient temperature to 1000°C. Dense bars were formed by pressing into a cylindrical shape having the dimensions of 6 mm diameter x 33 mm length at a hydraulic pressure of 170 MPa, then sintered at 1200-1300°C for 24h. The as-sintered bars were then cut to a length of 25mm. Lightweight ceramic bars, made by the polymer powder and polymer foam techniques, with the dimensions of 5 mm x 5 mm x 25 mm were used to measure the CTE.

3.6 Mechanical Properties

To characterize the fracture behavior and mechanical properties, the tension, compression, and bending strength were measured using an Instron model 4204 testing machine with a capacity of 4500 N. The testing was done at ambient temperature at a relative humidity of 85%-95%.

3.6.1 Tensile Strength

Lightweight CMZP and ZrO_2 specimens with dimensions of 6 mm x 10

mm x 90 mm were prepared. The specimens were attached to aluminum blocks using epoxy as illustrated in Fig. 3.2. The tensile strength of the specimens was determined at a constant crosshead speed of 0.5 mm/min[45].

3.6.2 Compressive Strength

Specimens having the dimensions of 12.5 mm x 50 mm x 50 mm were placed between two 130 mm diameter x 40 mm thick stainless-steel disks. The load-bearing surfaces of the specimens were parallel (determined by a level) to both the top and the bottom disks. The compressive strength of the specimens was determined at a constant crosshead speed of 0.6 mm/min (ASTM C 165-83, Measuring Compressive Properties of Thermal Insulation).

3.6.3 Flexural Strength

Specimens with the dimensions of 5 mm x 12.7 mm x 100 mm were tested in three-point-bending with a span of 50 mm and with a constant crosshead speed of 1.27 mm/min (ASTM C 203-85 Breaking Load and Flexural Properties of Block-Type Thermal Insulation). The flexural strength or MOR was calculated by the following equation:

$$\text{MOR (MPa)} = \frac{3\,P\,L}{2\,b\,d^2} \qquad (3.3)$$

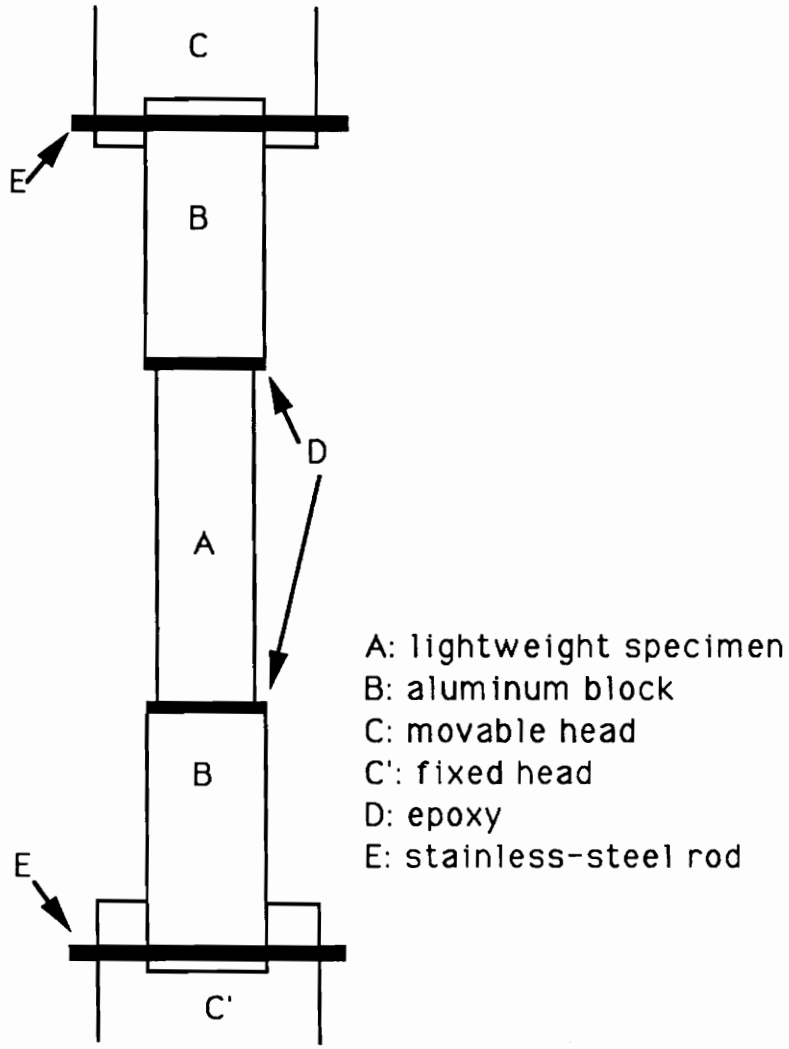

Figure 3.2 Lightweight tensile specimen.

where P = Load at fracture (N)

L = Span (50 mm)

b = Width of the specimens (mm)

d = Thickness of the specimens (mm)

3.6.4 Young's Modulus

Lightweight CMZP ceramics made by the polymer powder method were cut into 12.7 mm x 50 mm x 50 mm by using a diamond saw. The Young's modulus of the specimens was measured by Mr. Steven Warfeld in the Engineering Science and Mechanics Department of VPI & SU. The Young's modulus was calculated by:

$$E = \frac{d V^2}{g} \left[\frac{(1+\nu)\ (1-2\nu)}{(1-\nu)}\right] \qquad (3\text{-}4)$$

where V is the sound velocity and g is 386 in/sec^2.

3.7 Thermal Conductivity

Dense CMZP ceramics [(ρ/ρ_s) = 0.94] having dimensions of 3 mm thick x 10 mm in diameter and an average grain size 10 μm were coated with a thin layer of gold having thickness of 1000Å in both sides. The thermal diffusivity of the specimen was measured by Dr. D.P.H. Hasselman at the Advanced High-Temperature Materials Laboratory. The thermal conductivity of the specimen was determined by the product of bulk density, specific heat[40], and thermal diffusivity.

3.8 Thermal Shock Resistance

The specimens having dimensions of 5 mm x 12.7 mm x 100 mm were quenched in air after 10 min at temperatures from 200°C to 1500°C. Then broken in three-point bending as described in Section 3.6.3.

3.9 Corrosion Testing

The corrosion tests were performed by immersing lightweight CMZP samples made by the polymer foam method with a relative density of about 0.35 in aqueous hydrochloric and nitric acids at a normality of 12.1 and 15.8, respectively. The specimens were weighed before and after corrosion.

CHAPTER 4. RESULTS AND DISCUSSION

4.1 Pore Structure of Lightweight CMZP Ceramics

The microstructure of lightweight CMZP ceramics is controlled by the processing technique. Figure 4.1 shows the structure of the polymer foam which consists of open pores with short interconnecting struts. The resulting lightweight CMZP ceramic, Fig. 4.2, which is formed using coarse CMZP powders with an average particle size of 3-5 μm, has circular pores and a pore structure consisting of open and closed pores with an average pore size of 300 μm interconnected to form a three-dimensional network. Defects such as holes and/or cracks formed in the struts between pores from the pyrolysis of the polymer substrates, as shown in Fig. 4.3. These defects can be reduced by using the fine CMZP powders (45 nm), as shown in Fig. 4.4. This is because the fine powders have better sinterability at elevated temperature in comparison to the coarse powders.

With the polymer powder method, the pore structure is more complex. Figure 4.5 shows two of the lightweight ceramics with different relative densities and pore sizes. In the case of lower relative density 0.50, there is a combination of large pores having an average pore size of 200 μm and small pores (20-30 μm) which interconnect forming a continuous phase. At a relative density of

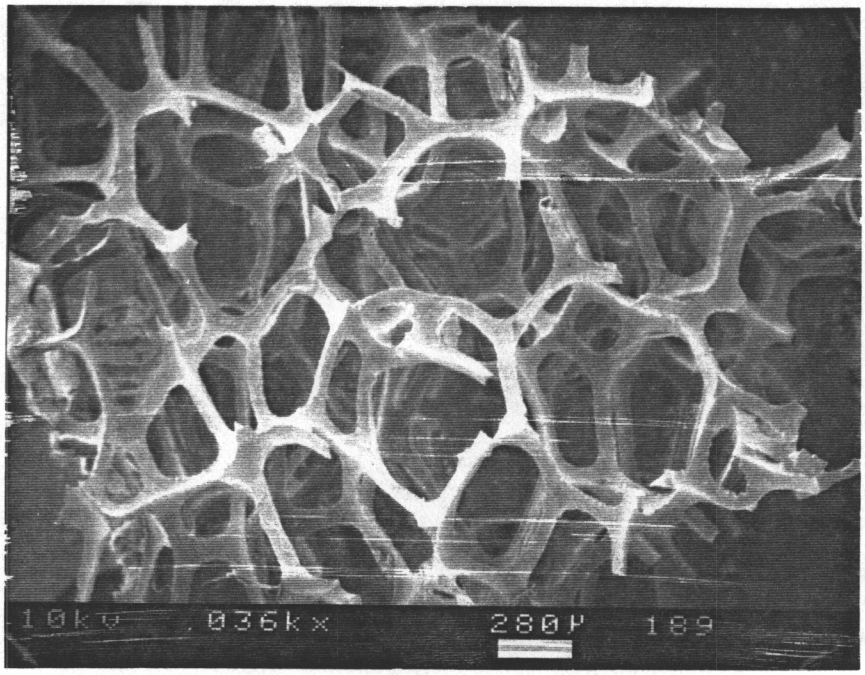

Figure 4.1 Microstructure of polymer foam

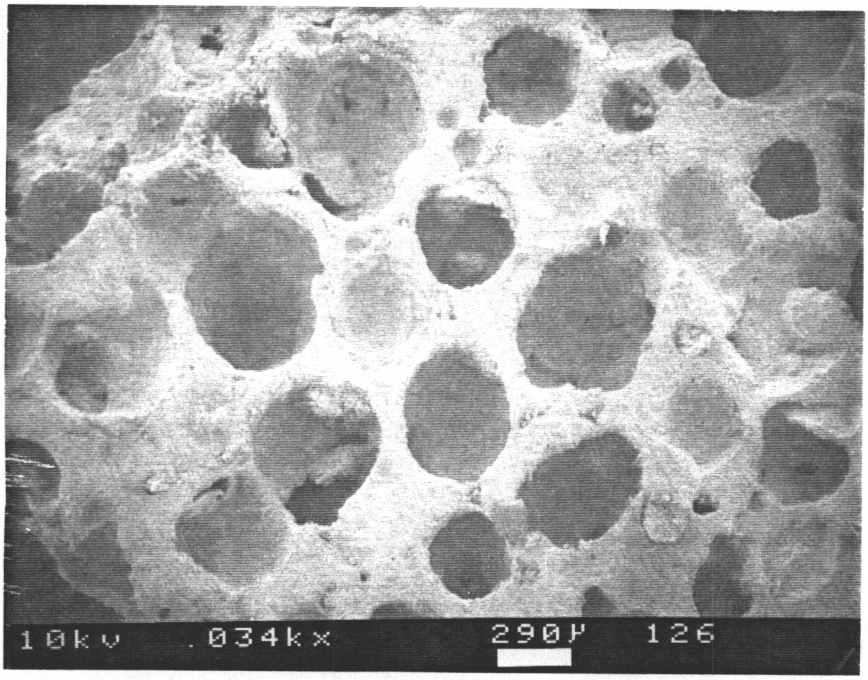

Figure 4.2 Microstructure formed by polymer foam method

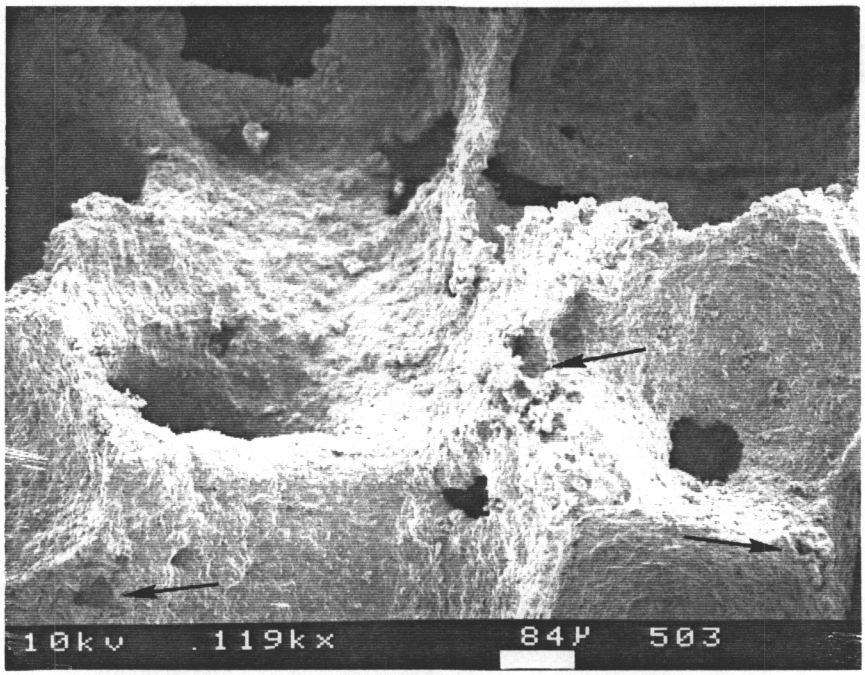

Figure 4.3 Defect structure between pores

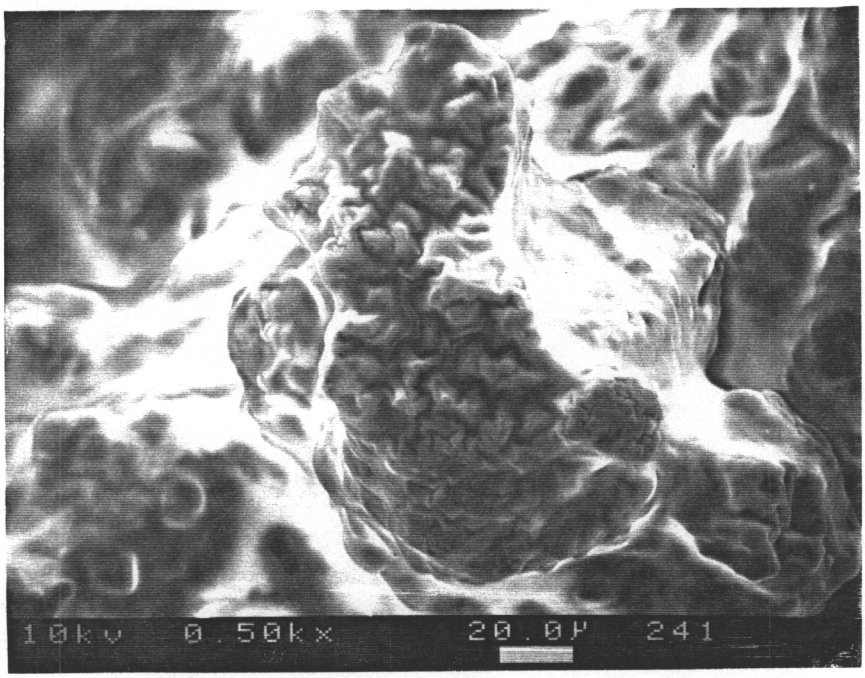

Figure 4.4 Elimination of the defect structure

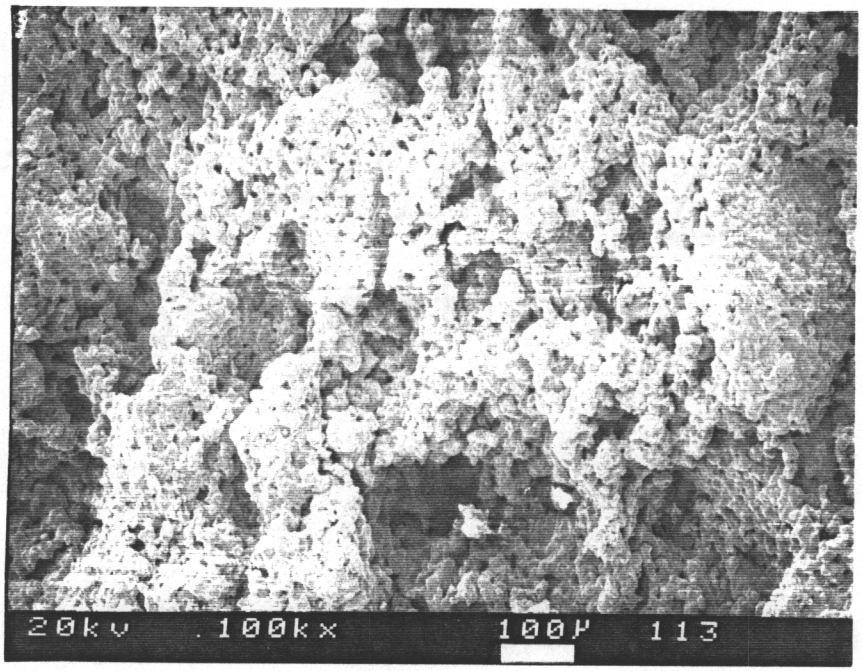

(a)0.50

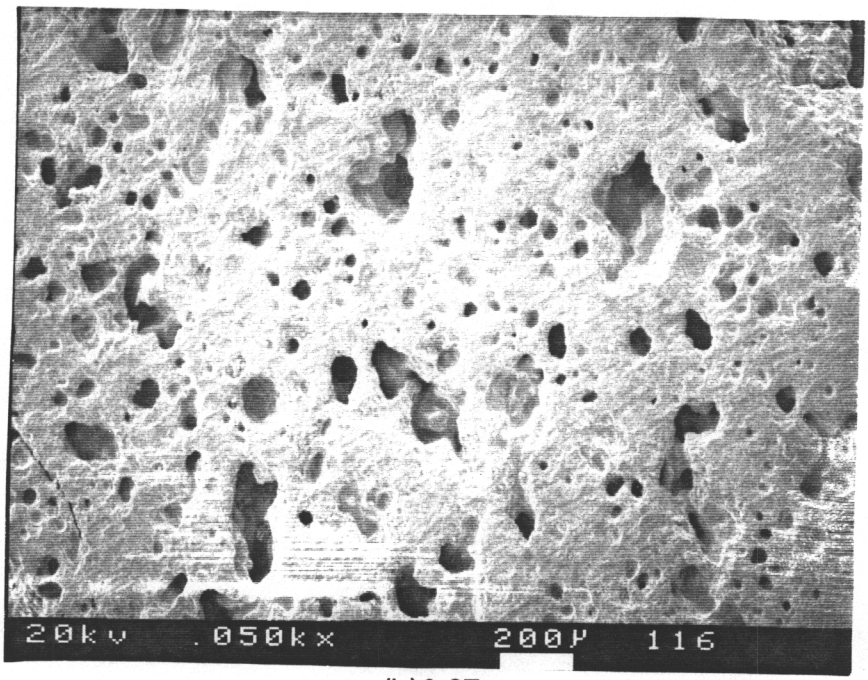

(b)0.67

Figure 4.5 Pore Structure of the lightweight CMZP ceramics were formed using the polymer powder method with relative densities of(a)0.50,(b)0.67.

0.67, the pores with an average size of 30-80 μm are isolated.

4.2 Permeability

The gas permeability is dependent on the microstructure of the lightweight CMZP ceramics, as shown in Fig. 4.6. The permeabilities are higher when made by the polymer foam method than by the polymer powder method, even at the same relative densities. This difference is because the foam method produces more and larger open pores. The permeability decreases with increasing relative density and exhibits a higher porosity dependence in the specimens prepared by the polymer foam method. This is because the percentage of open pores decreases rapidly as the relative density is increased.

Lightweight ceramics obtained from the polymer powder technique have lower values of permeability, indicating that the pore structure consists mainly of closed and small-sized pores. The closed pores do not affect the permeability, while small pores usually increase the pressure drop within the specimen, causing a decrease in the permeability. A transition in permeability of lightweight CMZP made by the polymer powder method is observed at a relative density of approximately 0.63 (Fig. 4.7). This transition can be explained by the percolation theory proposed by McCullough[46], that at low fraction of porosity the pores are isolated, as the porosity increases to a critical value, the amount of the isolated pores is increased and begin to connect to form an open channel which in turn rapidly increases the gas permeability.

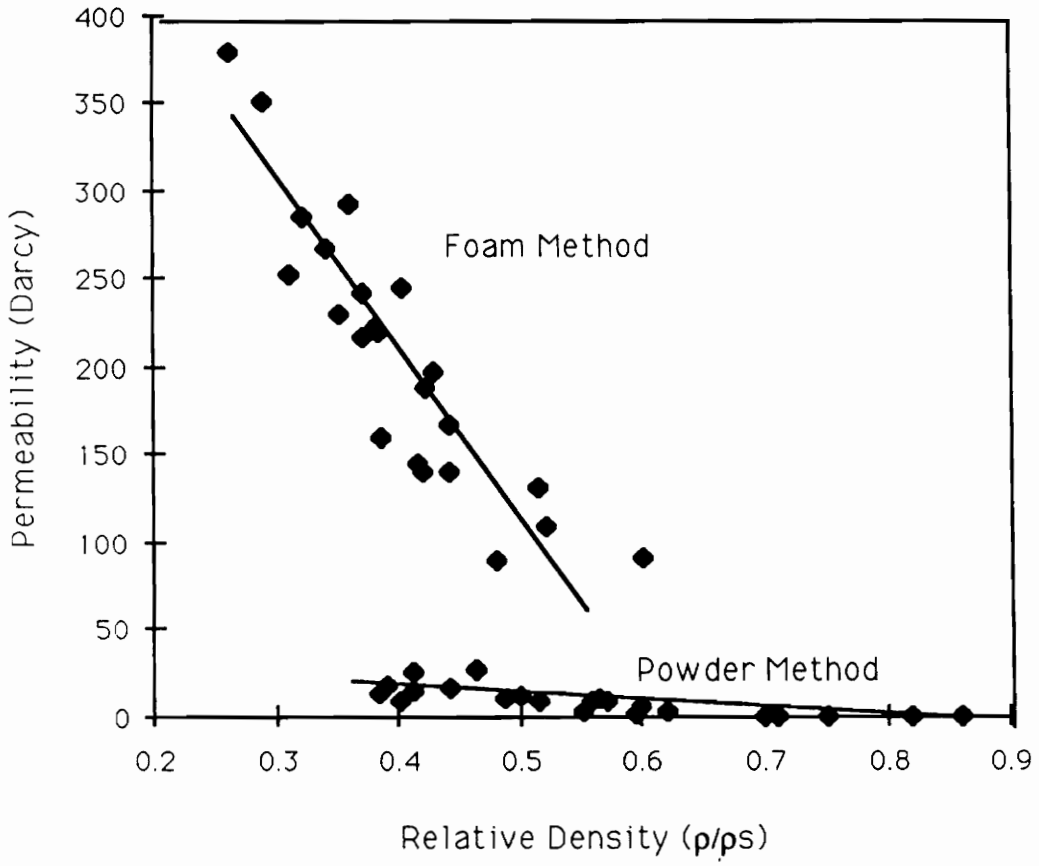

Figure 4.6 Permeability of lightweight CMZP as a function of relative density.

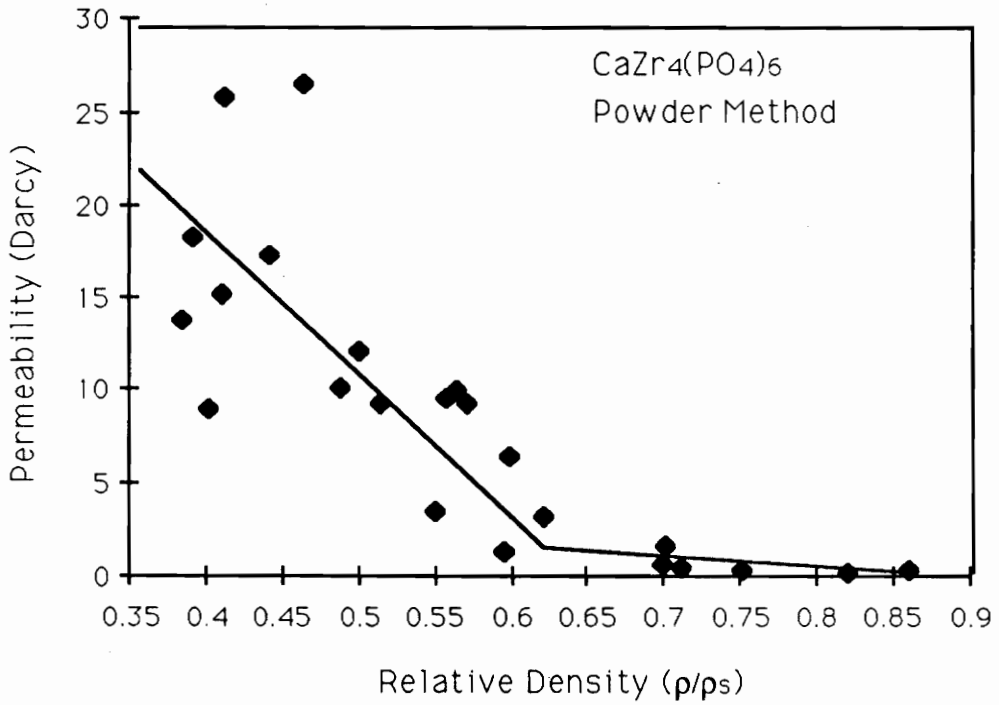

Figure 4.7 A transition in permeability indicates the pore structures changed.

4.3 Thermal Expansion

4.3.1 Effect of Porosity

The effect of porosity [$p = (1-(\rho/\rho_s))x100\%$] on CTE is illustrated in Fig. 4.8. The CTE of lightweight CMZP ceramics, made using the polymer powder and polymer foam methods, is independent of the porosity, which is consistent with the results of Coble et al in porous Al_2O_3[39].

4.3.2 Effect of Composition

In Fig. 4.9, the bulk expansion of lightweight CMZP, prepared by the polymer powder method with a relative density 0.42, exhibits a variation from negative CTE when x=0.0-0.2 to positive CTE when x=0.3-0.5. From the crystallographic point of view, when x=0.0, i.e., $CaZr_4(PO_4)_6$, the **a**-axis contracts ($\alpha_a<0$) upon heating, while the **c**-axis expands ($\alpha_c>0$), and the bulk expansion behavior is dominated by the **a**-axis[1]. Van Aken[40] investigated the thermal expansion of CMZP ceramics using high-temperature X-ray diffraction and found that the expansion in the **c**-axis direction is decreased as Mg content is increased. On the other hand, the contraction in the **a**-axis direction is decreased, and approaches zero when x=0.4. Therefore, the bulk expansion

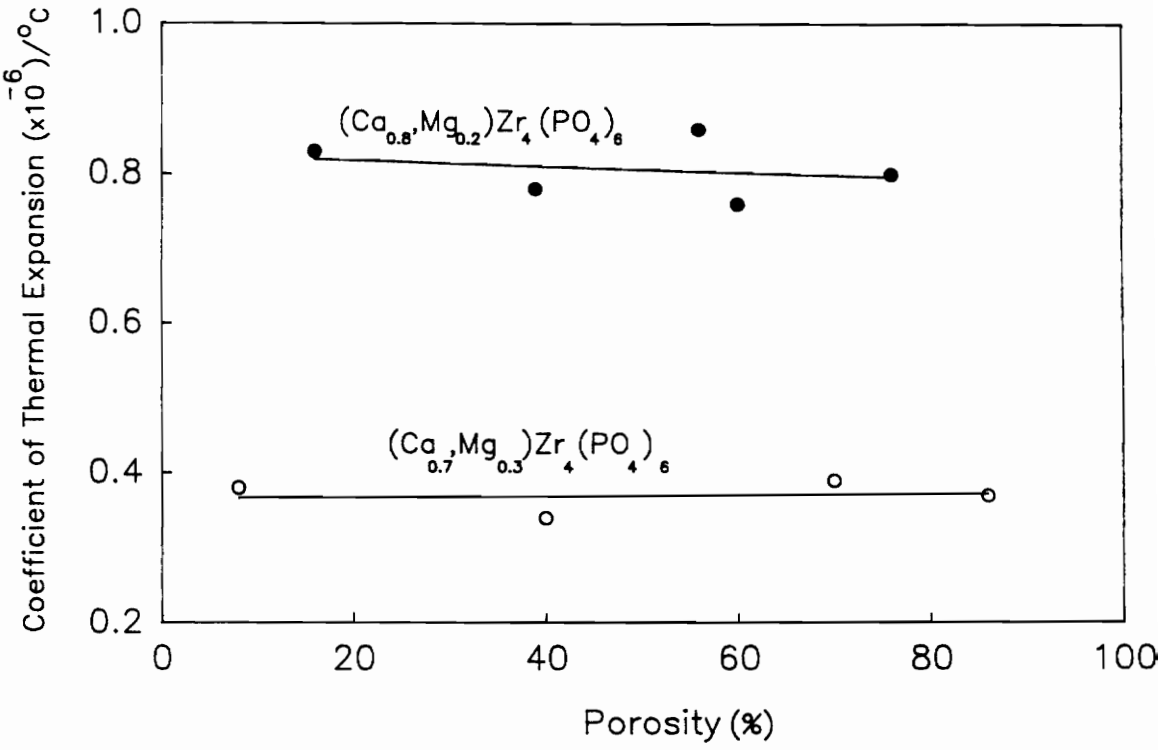

Figure 4.8 Effect of porosity on CTE of CMZP ceramics.

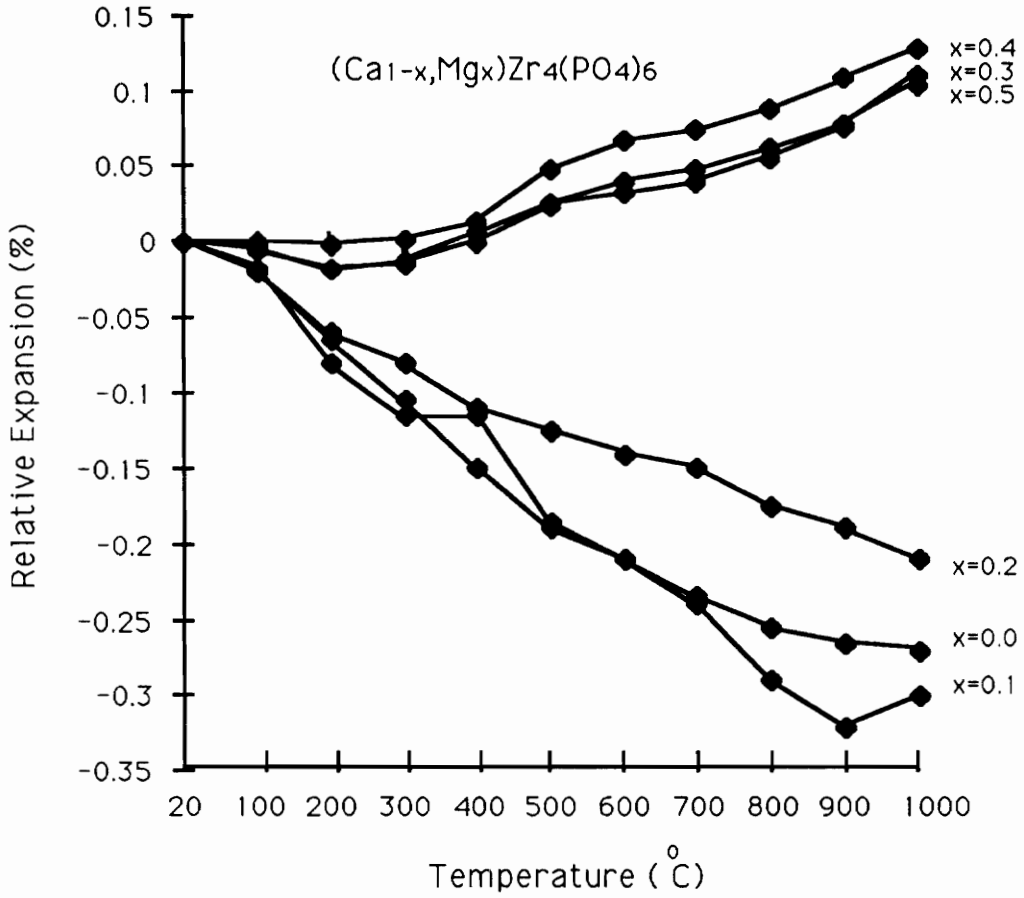

Figure 4.9 Expansion of lightweight CMZP ceramics as a function of composition and temperature.

of the **c**-axis becomes more pronounced as the Mg content increases and results in a positive CTE, which is consistent with experimental observations. At the same time, TEA is reduced as the Mg content increases.

4.3.3 Effect of Grain Size

The CTE of lightweight CMZP ceramics, made using the polymer powder method with a relative density of 0.45, varies with Mg content for both the fine and the coarse grain CMZP powders (Fig. 4.10). These results indicate that grain size may have an effect because the CTE values are different for the same composition.

The grain-size dependence of the CTE at different compositions is presented in Fig. 4.11. In the case of $CaZr_4(PO_4)_6$, i.e., x=0.0, the CTE changes from a positive value to near-zero, then to a negative value as the grain size increases. It appears that the CTE of the CMZP ceramics for x=0.3 and x=0.4 will change to zero or even negative at grain sizes larger than 6 μm (Fig. 4.11), which is due to the reduction of TEA resulting in larger critical grain size[15]. This variation in CTE can be explained in terms of the formation of microcracks as proposed by Yamai et al[42], who indicated that the thermal expansion coefficient decreased because of the increase in the microcrack content with grain growth. However, where there are small grains and no microcracking occurs,(Fig.4.12), the CTE also decreases with increasing grain size, implying

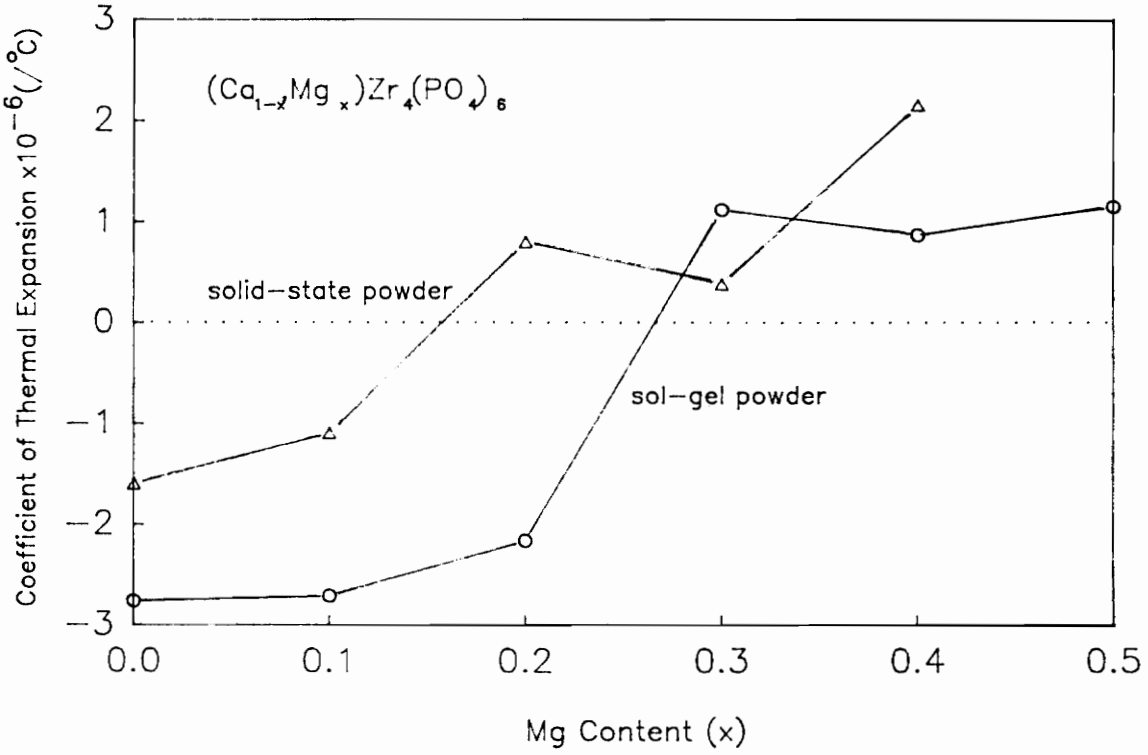

Figure 4.10 CTE of lightweight CMZP ceramics versus Mg.

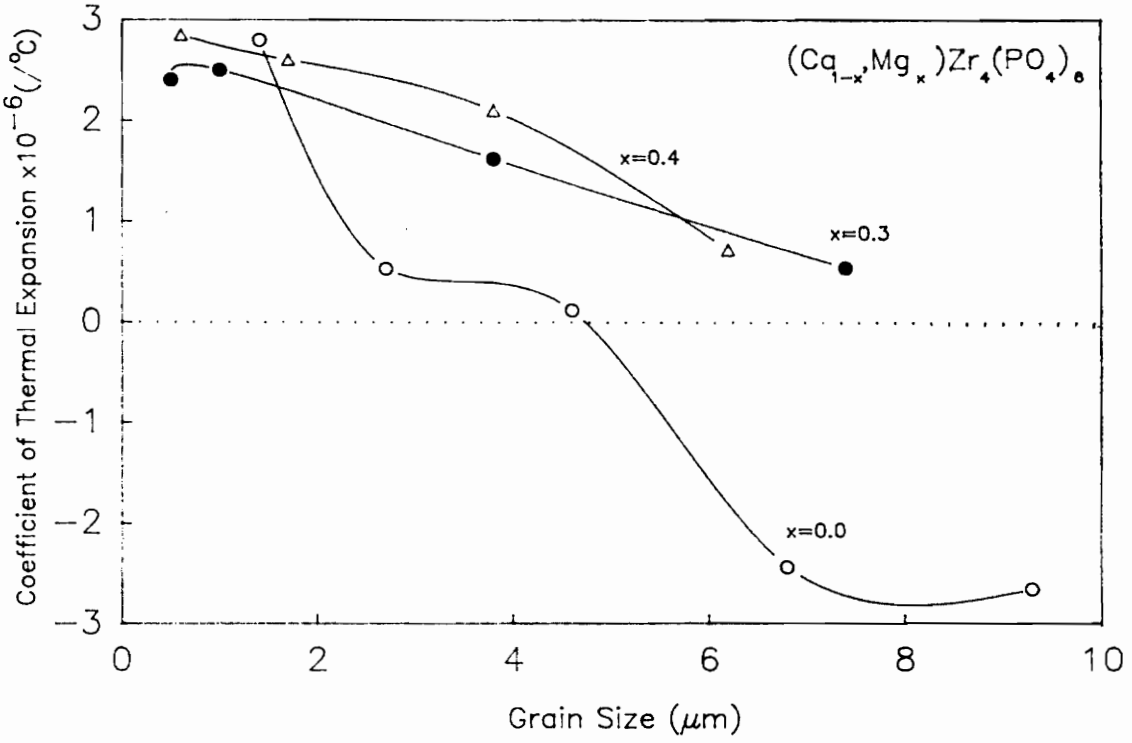

Figure 4.11 CTE of lightweight CMZP ceramics as a function of composition and grain size.

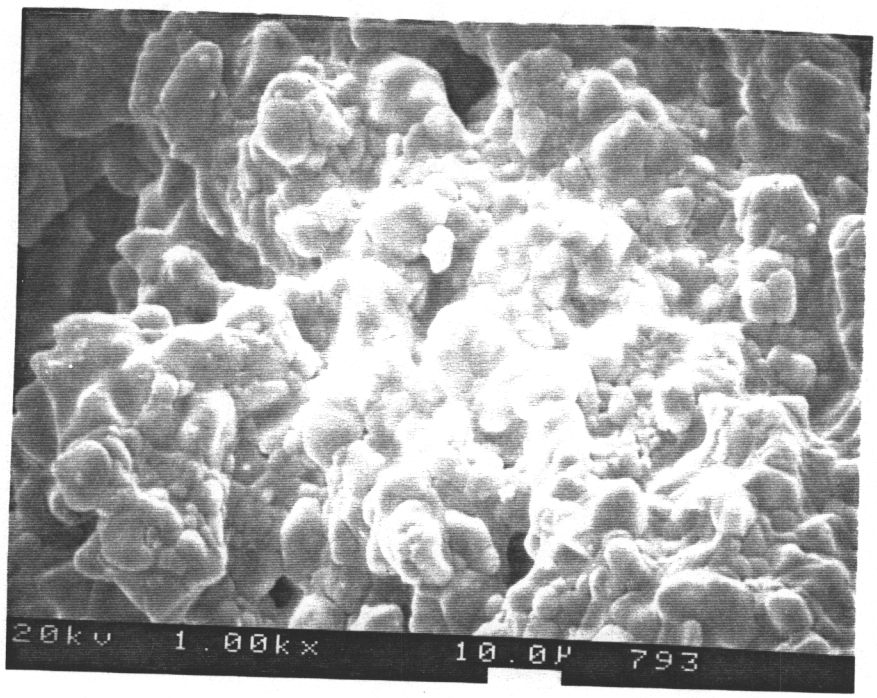

Figure 4.12 Microcrack-free lightweight CMZP with x=0.3.

other factors such as grain boundaries and impurities may affect the expansion.

4.3.4 Thermal Expansion Hysteresis

Figure 4.13 shows the expansion hysteresis of lightweight CMZP made by the polymer powder method with a relative density of 0.75. A large thermal expansion hysteresis appears in the large-grain sample, i.e., the cooling curve falls substantially below the heating curve. In contrast, the thermal expansion hysteresis is reduced with a smaller grain size. These expansion curves substantiate the microcracking reoccurrence and recombination concepts proposed by Buessem[43], who stated that upon heating the crack width decreases linearly. The recombination occurs spontaneously at certain temperatures where the attractive force, i.e., London-Van der Waals force, is large enough to close the crack. Upon cooling, when the temperature is sufficiently different from the critical temperature, internal cracks form causing a hysteresis effect. The expansion curves are analogous to the trends in grain-size effects on the thermal expansion of Nb_2O_5 reported by Manning et al[44], who pointed out that the hysteresis effect is more pronounced in large-grained materials.

In Fig. 4.14, the expansion of the lightweight CMZP, made by the polymer powder method with a relative density of 0.75 and grain size of 4.6 μm, exhibits different hysteresis effects with thermal cycling. The variations in the hysteresis of lightweight CMZP are consistent with the concepts proposed by Kuszyk et

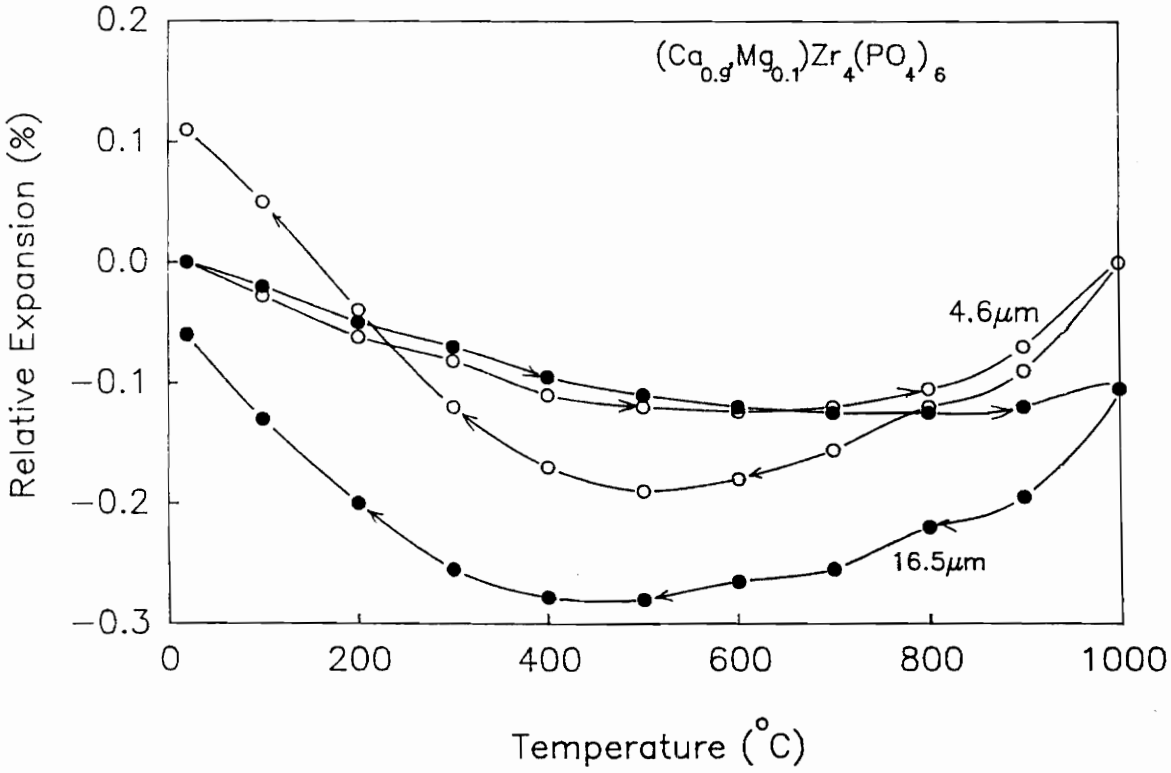

Figure 4.13 Effect of grain size on expansion hysteresis of CMZP.

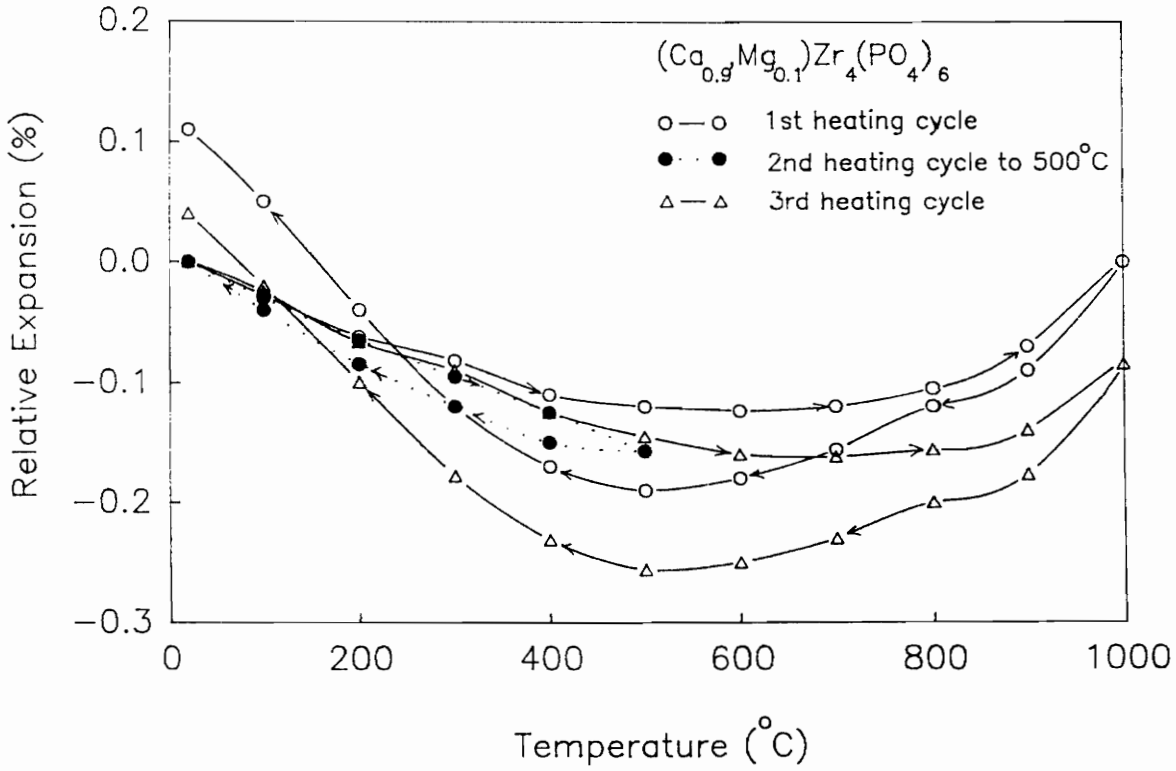

Figure 4.14 Thermal expansion hysteresis of lightweight CMZP ceramics with a grain size of 4.6 μm.

al[13] who showed that the thermal expansion anisotropy stress is accompanied by a strain field and stored elastic strain energy. If microcracks begin to form at some temperatures, e.g., above 500°C in this case, part of the stored elastic strain energy will be converted to the fracture surface energy of the microcracks which results in an increased specimen length as in the first thermal cycle. Once the microcracks form, the internal stresses within the material are decreased, and will be further decreased by extending the microcrack fracture surface, which again increases the length of the specimen, as in the third thermal cycle. Moreover, as compared to the first thermal cycle, the third cycle exhibits a larger hysteresis loop which is evidence of the formation of new fractured surfaces.

4.4 Thermal Conductivity

Due to high inaccuracy in measuring the thermal conductivity of low density porous CMZP using the laser-flash technique, dense CMZP was studied. In Fig. 4.15, CMZP ceramics, having an average grain size 10 μm and a relative density of 0.94, exhibit values of thermal conductivity lower than dense ZrO_2[18], a conventional thermal barrier material. The thermal conductivity is decreased with increasing Mg content. One reason is because the CMZP has a more complex crystal structure which reduces the mean free path of the thermoelastic waves. The presence of microcracks observed in these samples act as a barrier

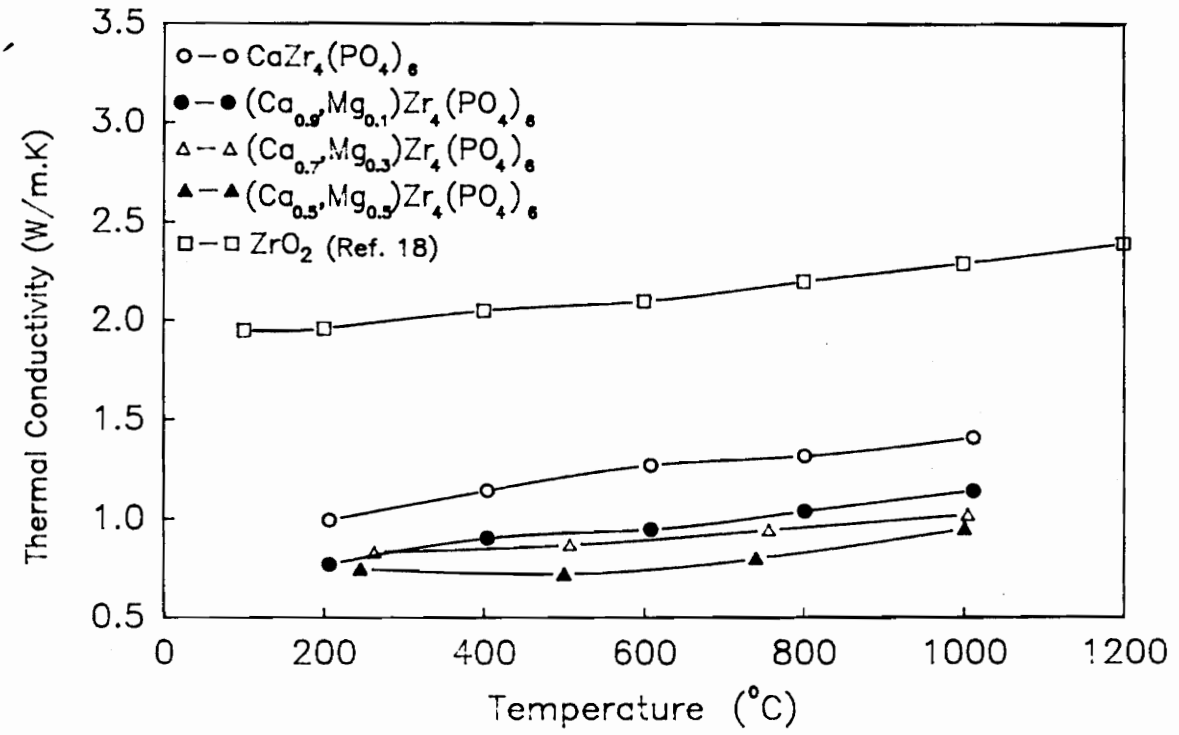

Figure 4.15 Thermal conductivity of dense CMZP ceramics.

to the thermoelastic waves further reducing the mean free path and resulting in lower values of thermal conductivity.

The effect of Mg content on the thermal conductivity is caused by decreasing of lattice volume resulting from substitution of smaller Mg^{+2} cations[40]. This substitution deforms the framework structure increasing the disorder of the structure[10] hence, reduces the thermal conductivity.

4.5 Mechanical Properties

For lightweight CMZP ceramics, the cracks tend to propagate along the largest pores or the most serious defects such as microcracks. Hence, the strength usually does not reflect the average properties, but rather the largest defects in the microstructure.

4.5.1 Tension

The tensile strength of lightweight CMZP ceramics having compositions of x=0.0 to x=0.3, increases with relative density and appears to be independent of the composition, as shown in Fig. 4.16. It is apparent that the tensile strength is directly related to the connected area of the solid network[32], since there is no obvious strength difference between the fabrication methods.

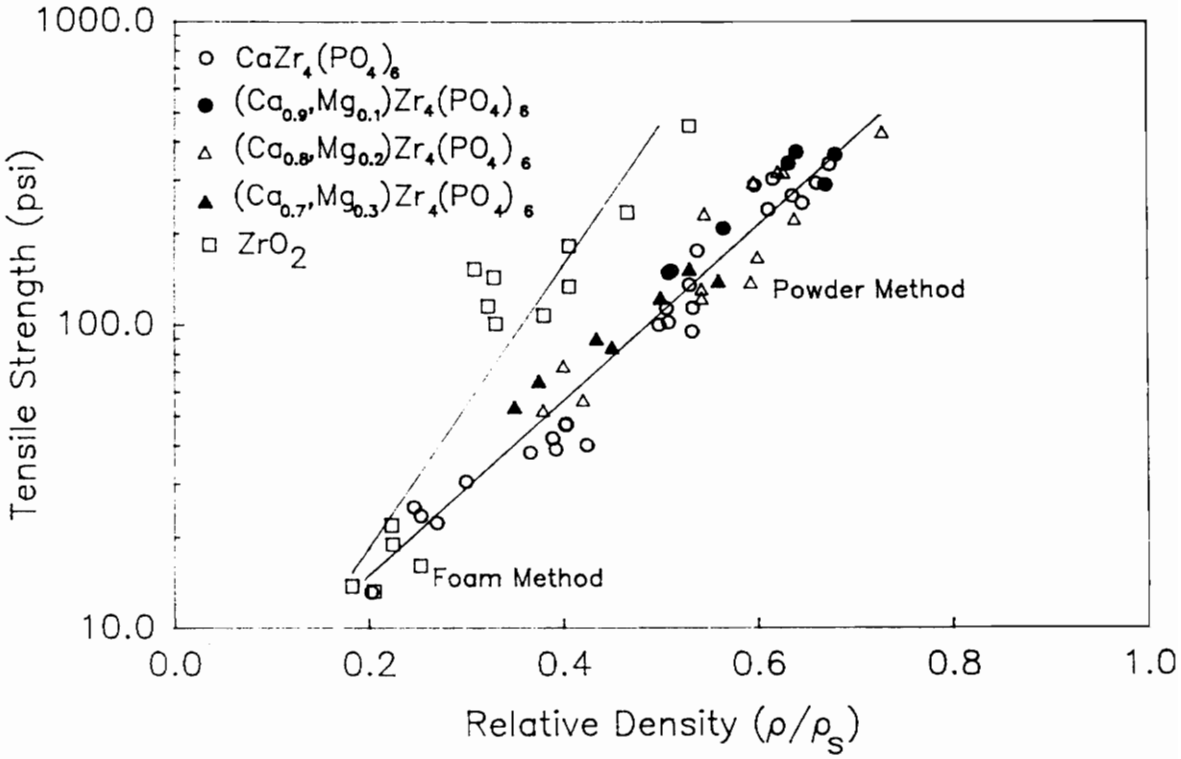

Figure 4.16 Tensile strength versus relative density for lightweight ceramics.

In Fig. 4.16, the tensile strength as a function of relative density of lightweight CMZP ceramics follows a straight line by the method of least squares with a correlation coefficient of 0.93 and a standard deviation of 0.08. It can be written as

$$S_t = 3{,}300\ e^{-6.7p}\ (\text{psi}) \qquad (4\text{-}1)$$

where S_t is the tensile strength of lightweight CMZP ceramics.

For lightweight ZrO_2 made by the polymer powder method, the resulting porosity dependence of tensile strength is

$$S_t(ZrO_2) = 96{,}300\ e^{-10.7p}\ (\text{psi}) \qquad (4\text{-}2)$$

The tensile strength of fully dense ZrO_2, 96,300 psi is close to that measured by Noguchi et al[45], who reported the tensile strength of ZrO_2 is 94,300 psi. Figure 4.16 shows lightweight ZrO_2 having a higher strength than lightweight CMZP at the same porosity, which is due to the formation of microcracks within the solid network of CMZP and to the larger CMZP powder size; thus reduces the strength. If based on bulk density the lightweight CMZP ceramics exhibit higher tensile strength as illustrated in Fig. 4.17. This is because for the same bulk density, lightweight ZrO_2 contains higher porosity than that in lightweight CMZP, since the density of ZrO_2 is nearly twice as that of CMZP,

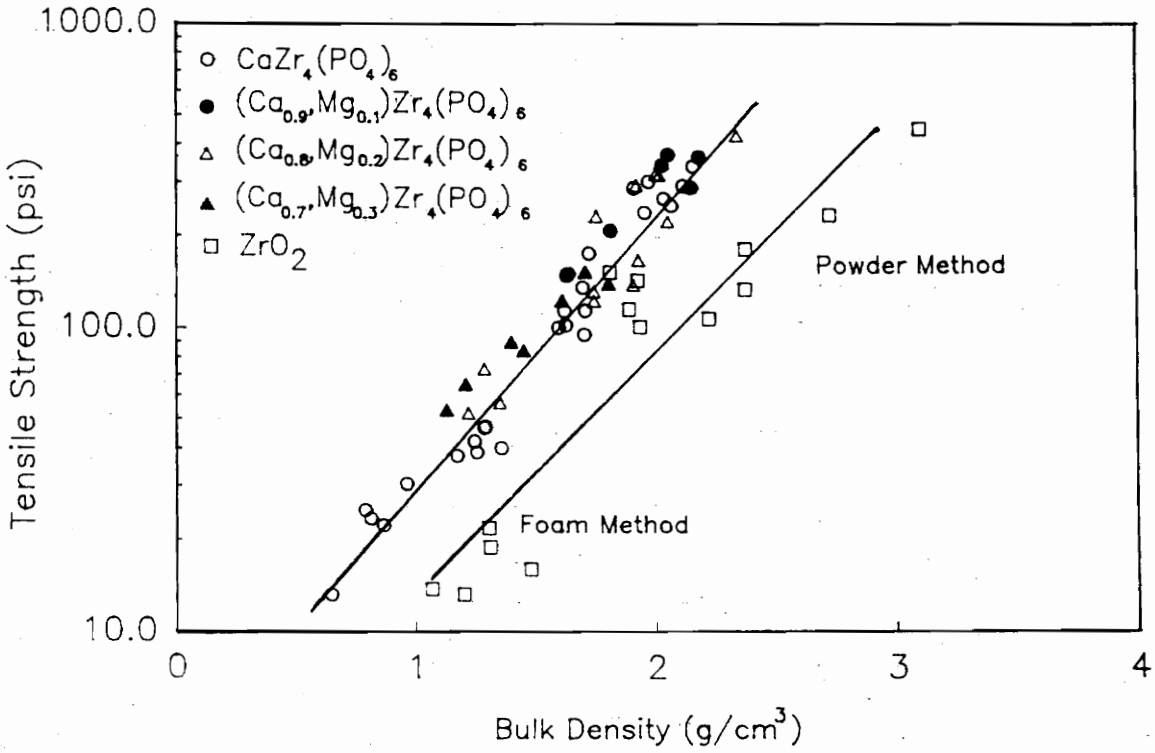

Figure 4.17 Tensile strength versus bulk density for lightweight CMZP and ZrO_2.

and results in a less connected area of the solid network; hence reduce the strength. Therefore, lightweight CMZP ceramics may be suitable for applications where the weight is a critical factor.

4.5.2 Compression

Typical compressive stress-strain curves of the lightweight CMZP ceramics exhibit three regimes of behavior: linear elastic, collapse, and densification, in Fig. 4.18. The lightweight CMZP ceramics made by the polymer powder method fail rapidly because the stress concentrates near large and complex pores[32] (as in Fig. 4.5(a)) which leads to catastrophic failure once the compressive stress exceeds the crushing strength. In contrast, the lightweight CMZP ceramics made using the polymer foam method fail stepwise in the collapse mode, where the compressive stress is shared by cell-edge bending and cell-wall stretching[30].

The dependence of the compressive strength on the relative density of lightweight CMZP ceramics is shown in Fig. 4.19. A transition in the compressive strength occurs at a relative density of 0.35, due to the change in forming technique. This shows that the compressive strength is strongly affected by pore structure. The relations between the compressive strength and relative density can be expressed in terms of porosity using the method of least squares:
for polymer powder method,

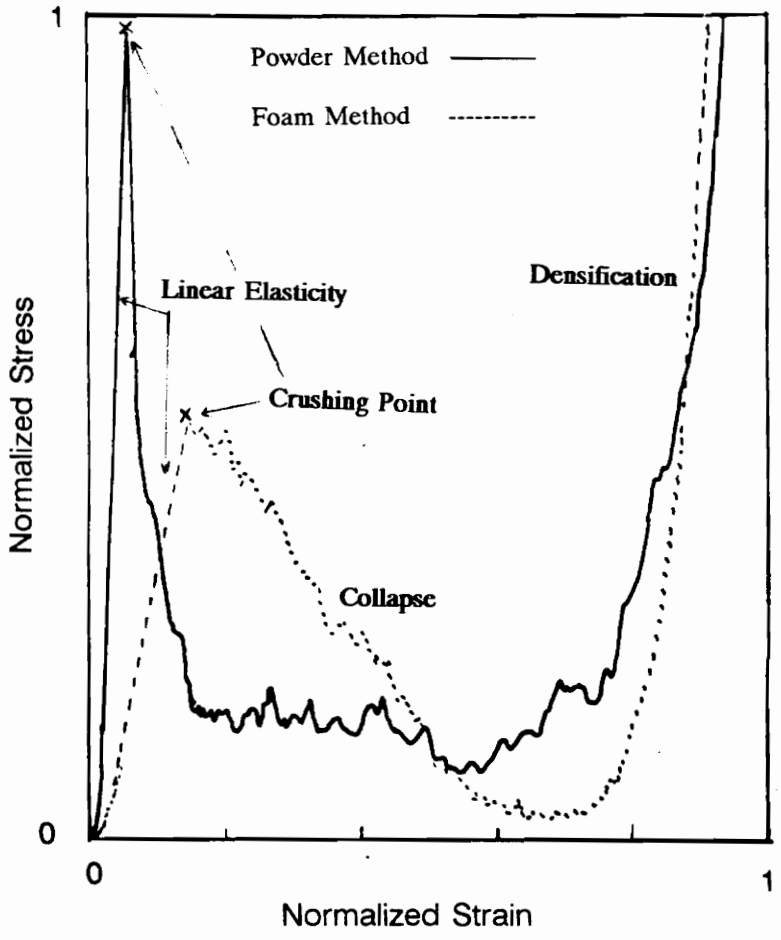

Figure 4.18 Compressive stress-strain curves of lightweight CMZP ceramics.

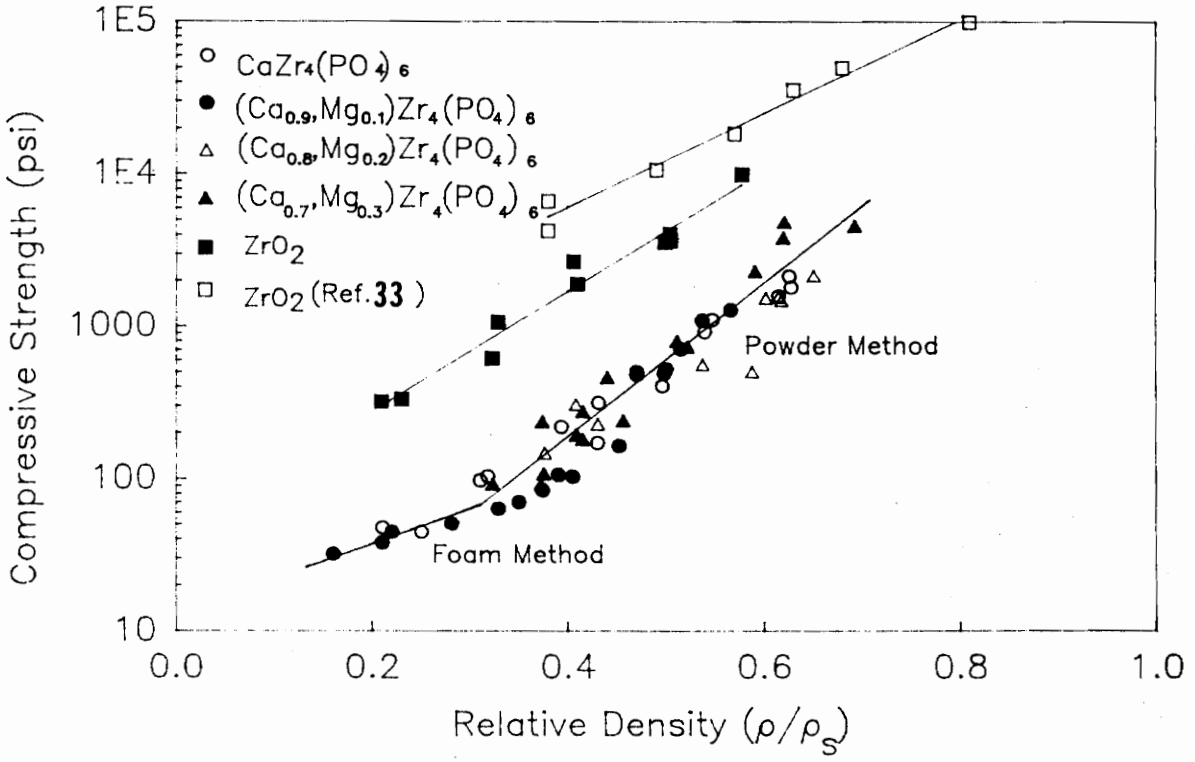

Figure 4.19 Compressive strength versus relative density for lightweight CMZP and ZrO_2.

$$S_c = 140{,}000\ e^{-11.0p}\ (psi) \quad (4\text{-}3)$$

for polymer foam method,

$$S_c = 1800\ e^{-4.8p}\ (psi) \quad (4\text{-}4)$$

which have correlation coefficients of 0.95, 0.96, and standard deviations of 0.04, 0.03, respectively, and S_c is compressive strength.

The b value in eq.(4-3) is larger than that in eq.(4-4), indicating substantial inhomogeneity of spatial distribution and shape of pores present in lightweight CMZP ceramics made by the powder method, which is consistent with the SEM results and also agrees with the experimental results of Gannon[36] and Kundsen[37].

The lightweight CMZP ceramics exhibit a lower value of compressive strength than lightweight ZrO_2 (Fig. 4.19) which can be expressed as

$$S_c(ZrO_2) = 400{,}000\ e^{-9.1p}\ (psi) \quad (4\text{-}5)$$

This is close to that presented by Ryshkewitch[33] for ZrO_2 foam with a uniform pore size of 300 μm. His strength-porosity relation is

$$S_c,(ZrO_2) = 420{,}000\ e^{-7.0p}\ (psi) \quad (4\text{-}6)$$

The difference in b value between eq.(4-5) and (4-6) indicates a more inhomogeneous porosity exists in ceramics made by the polymer powder method.

On the basis of bulk density, the compressive strength of the lightweight CMZP ceramics is comparable to that of the lightweight ZrO_2, as shown in Fig. 4.20, which can be explained as that in the case of tension where higher porosity content can be achieved in ZrO_2 than that in CMZP for the same bulk density.

4.5.3 Modulus of Rupture

In Fig. 4.21, the MOR of lightweight CMZP ceramics appears to be independent of the composition. No obvious strength variation is observed between the fabrication methods, indicating that the MOR is insensitive to the pore structure but is directly affected by the connected area of the solid network as that in tension (Fig. 4.16). As shown, the relation of MOR and relative density can be expressed as porosity dependence using the method of least squares with a correlation coefficient of 0.92 and a standard deviation of 0.08, thus

$$MOR = 26{,}620\ e^{-9.00p}\ (psi) \qquad (4\text{-}7)$$

The MOR of lightweight CMZP ceramics approaches that of lightweight ZrO_2 (Fig. 4.21), which can be expressed as

$$MOR(ZrO_2) = 130{,}000\ e^{-11.1p}\ (psi) \qquad (4\text{-}8)$$

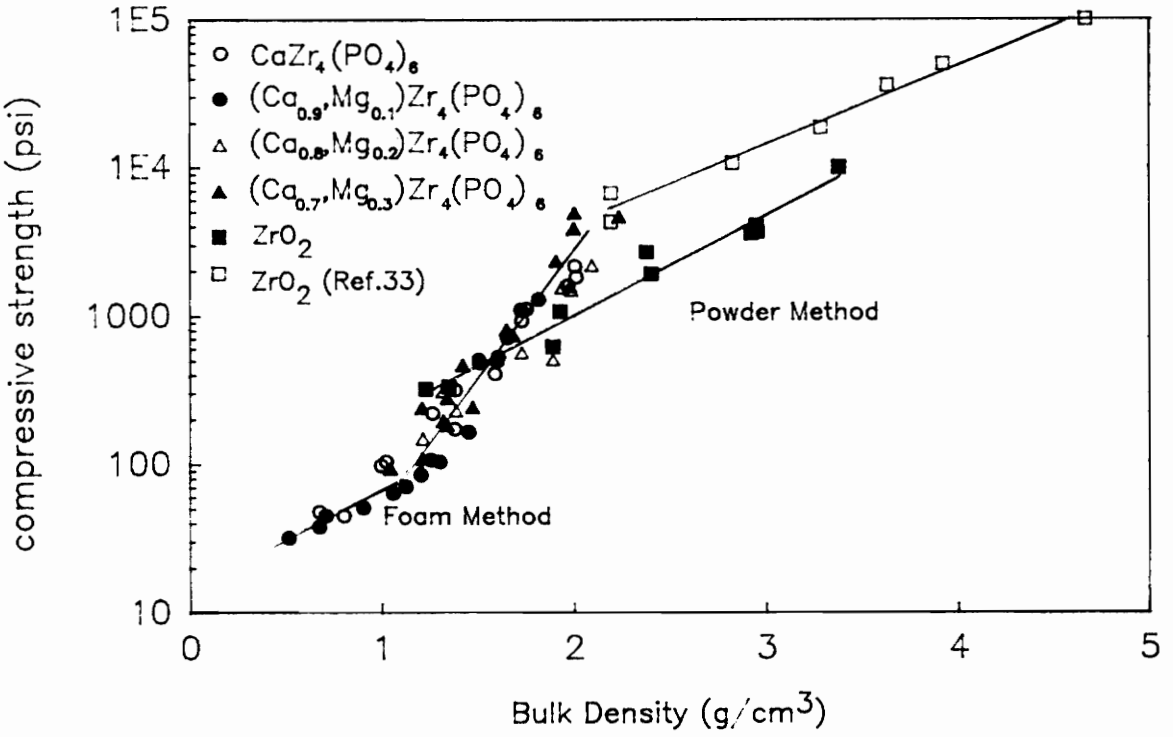

Figure 4.20 Compressive strength versus bulk density for lightweight CMZP and ZrO_2.

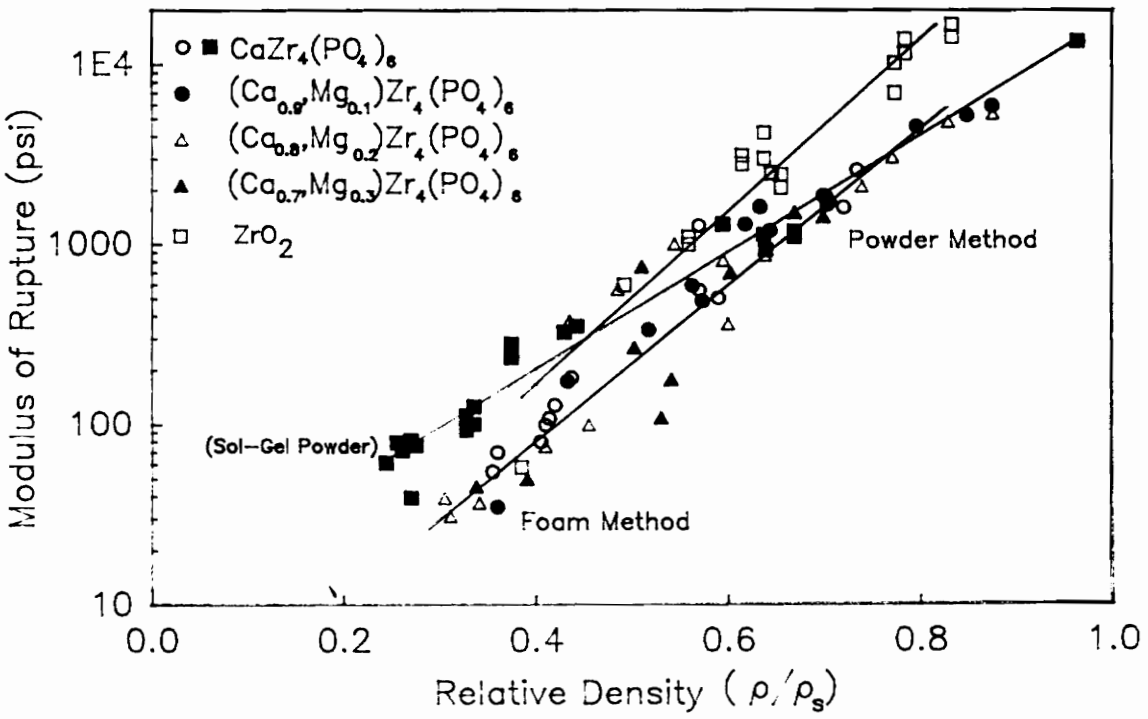

Figure 4.21 Effect of powder size and relative density on MOR of lightweight ceramics.

The particle size of CMZP powder also affects the MOR of the lightweight CMZP ceramics by changing the microstructure which has already been discussed in Section 4.1. The MOR of lightweight CMZP ceramics made using the fine powders (45 nm) is three to five times larger than those made using the coarse powders (3-5 μm) at relative densities between 0.22 and 0.42 and also have strength higher than that of lightweight ZrO_2. This difference in MOR is due to a reduction in the defects (Fig. 4.4). The relationship between MOR and porosity for the fine CMZP powders, having composition of x=0.0, is expressed as

$$MOR_{(\text{fine powder})} = 17{,}400\ e^{-6.7p}\ (\text{psi}) \qquad (4\text{-}9)$$

At a given bulk density, the MOR of the lightweight CMZP ceramics is higher than that of lightweight ZrO_2, Fig. 4.22, as that observed in tension. The similarity between tension and MOR is believed to be due to the same reason which has already been discussed in Section 4.5.1.

4.5.4 Young's Moduli

Figure 4.23 shows the exponential relation of relative density versus Young's moduli of lightweight CMZP and ZrO_2 ceramics, made by the polymer powder method. All the data, for each composition, can fit into a linear relation using the method of least squares:

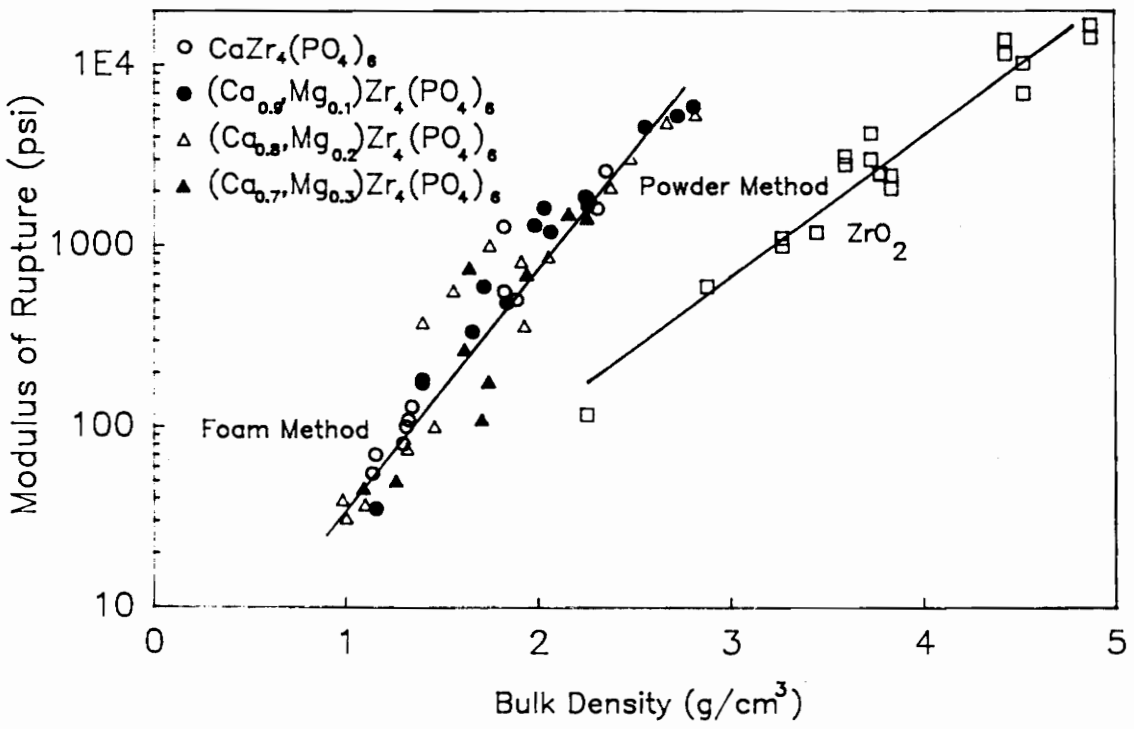

Figure 4.22 MOR versus bulk density for lightweight CMZP and ZrO_2.

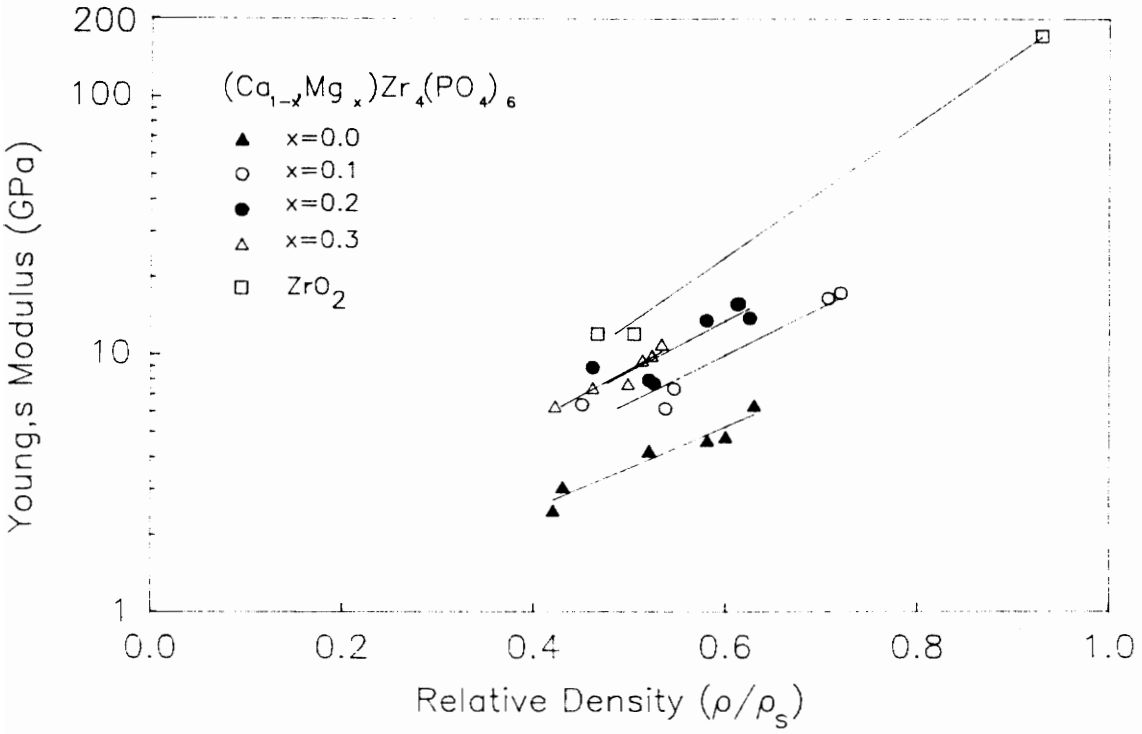

Figure 4.23 Young's moduli of lightweight CMZP ceramics are functions of porosity and compositions.

$$x=0.0, \quad E = 22.62\ e^{-3.7p}\ (GPa) \tag{4-10}$$

$$x=0.1, \quad E = 54.15\ e^{-4.2p}\ (GPa) \tag{4-11}$$

$$x=0.2, \quad E = 81.27\ e^{-4.5p}\ (GPa) \tag{4-12}$$

$$x=0.3, \quad E = 93.80\ e^{-4.7p}\ (GPa) \tag{4-13}$$

$$\text{for } ZrO_2, \quad E = 207.34\ e^{-6.6p}\ (GPa) \tag{4-14}$$

One explanation for the Young's moduli of dense CMZP ceramics increase with Mg content is due to the reduction of lattice volume by replacing larger Ca^{2+} cations with smaller Mg^{2+} cations[40]. This lattice volume reduction leads to a more rigid framework structure. Hence, a higher strength is required to separate adjacent atoms, which in turn results in higher values of Young's moduli.

4.5.5 Effect of ZnO on Strength

Figure 4.24 illustrates the effect of ZnO on the strength of lightweight CMZP ceramics with x=0.0-0.3. The lightweight CMZP ceramics presented in Fig. 4.24 were made by the polymer foam method with relative densities of 0.25 to 0.34 as noted in the figure. The tensile strength increases with ZnO content up to 1 wt%, then declines slowly with further addition of ZnO. This strength degradation is due to the formation of large grains (12-15 μm) resulting from higher ZnO content for the same processing conditions. Since the number of

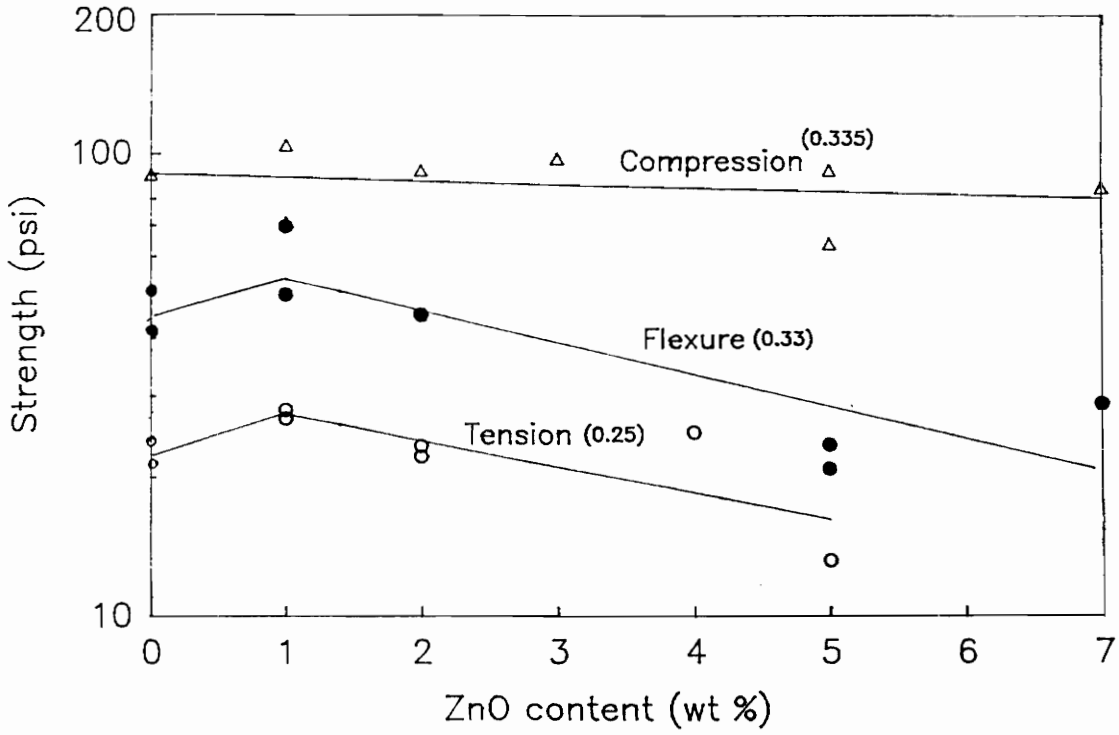

Figure 4.24 Variation in strength of lightweight CMZP ceramics with ZnO content.

microcracks increases with increasing grain size, the strength degradation reflects microstructure-related fracture.

In contrast, no significant variation in compression with increasing ZnO is observed, indicating the compressive strength is insensitive to the ZnO content for these relative densities.

4.6 Thermal Shock Resistance

The thermal shock resistance of lightweight CMZP ceramics, made by the polymer powder and polymer foam (ρ/ρ_s=0.25) methods, is illustrated in Fig. 4.25 and Fig. 4.26, where five to six specimens were measured at each temperature. As shown in Fig. 4.25, the strength of lightweight CMZP ceramics having different relative densities is nearly constant after quenching, which is attributed to their ultra-low coefficient of thermal expansion minimizing the internal stresses resulting from TEA.

At a relative density of 0.25 (Fig. 4.26), the strength is nearly constant after quenching, perhaps because of the initial low value of strength before thermal shock[25]. Moreover, in highly porous solids the internal stresses resulting from crystalline anisotropy can also be shared by the cell-edge bending and/or cell-wall stretching[30], resulting in an excellent thermal shock resistance as observed in the experiment.

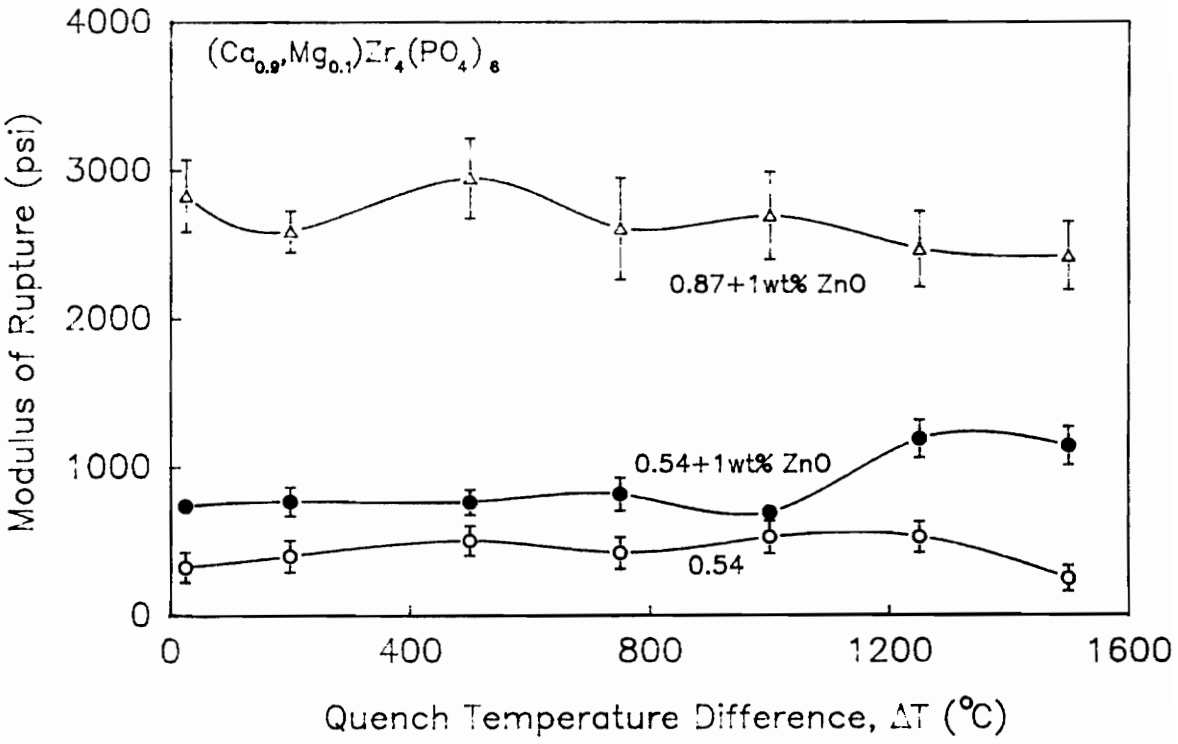

Figure 4.25 Thermal-shock resistance of lightweight CMZP for x=0.1.

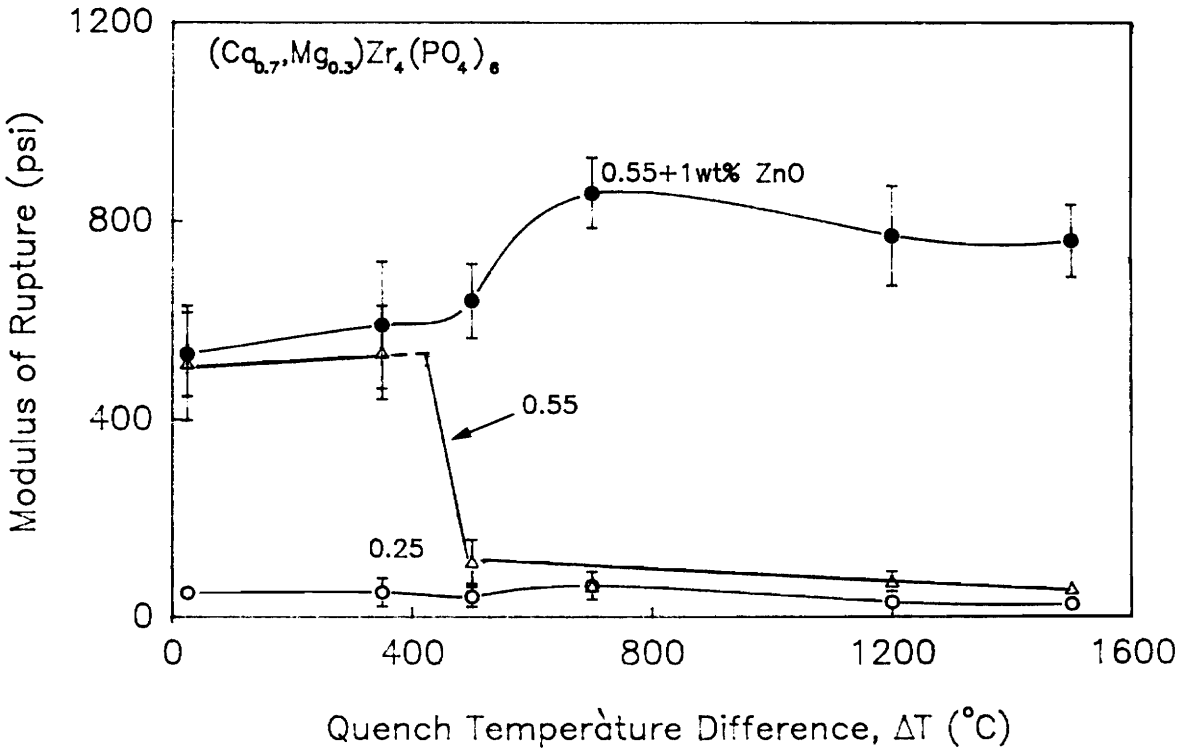

Figure 4.26 Thermal-shock resistance of lightweight CMZP for x=0.3.

However, the strength of the specimen ((ρ/ρ_s)=0.55) without ZnO decreases rapidly when quenched from about 500°C, but no strength degradation is observed in the specimens containing ZnO having the same relative density (Fig. 4.26). One explaination for this difference is attributed to the release of internal stresses due to crystalline anisotropy such as thermal expansion anisotropy and elastic anisotropy. These stresses are released by microcracking, especially in the system without ZnO where the grain size is large enough to nucleate microcracks along the grain boundaries (Fig. 4.27). Fracture cracks propagate within the solid network after the specimens were quenched from a critical temperature difference of about 500°C, decreasing the strength (Fig. 4.28). Once the cracks are formed, the strength decreases gradually even after severe thermal shock (Fig. 4.26), due to cracks propagating in a quasi-static manner[24]. The grain size in the system containing ZnO is small compared to the former system. This is due to the fact that these specimens were processed with a very short sintering time (10 min) at 1300°C. Therefore, less microcracks are expected in this system. Furthermore, a secondary phase, $Zn_3(PO_4)_2$, forms at the grain boundary and inhibits crack propagation. These effects combine to result in excellent resistance to thermal shock in this system.

As compared to Fig. 4.26, Fig. 4.25 shows a different strength behavior over a similar range of relative density (0.55 and 0.54 respectively) where no strength degradation can be observed. This is in conflit with that observed in Fig. 4.26. This is probably due in part to differences in extensibility (S_t/E), where

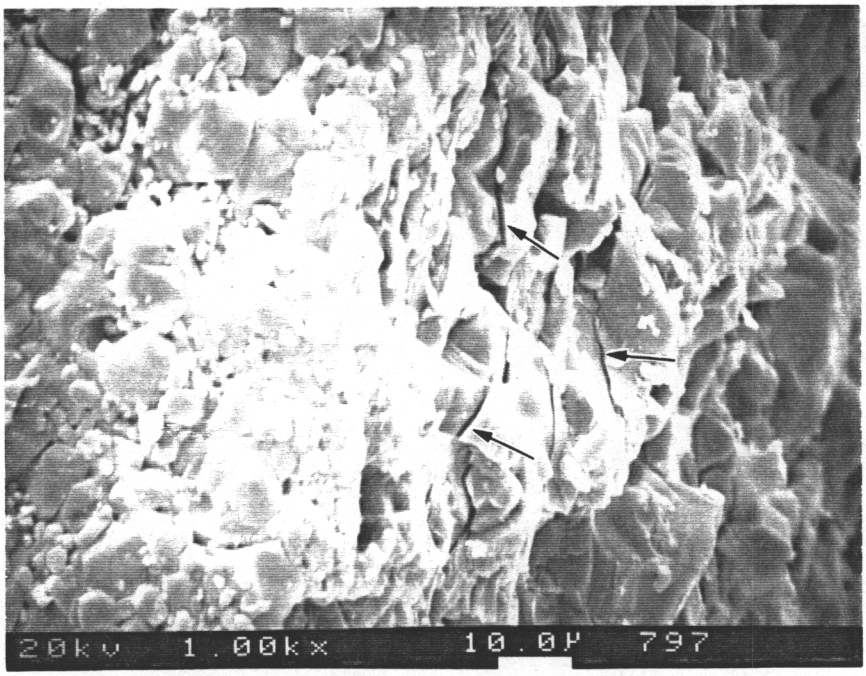

Figure 4.27 Microcracks on grain boundaries in CMZP.

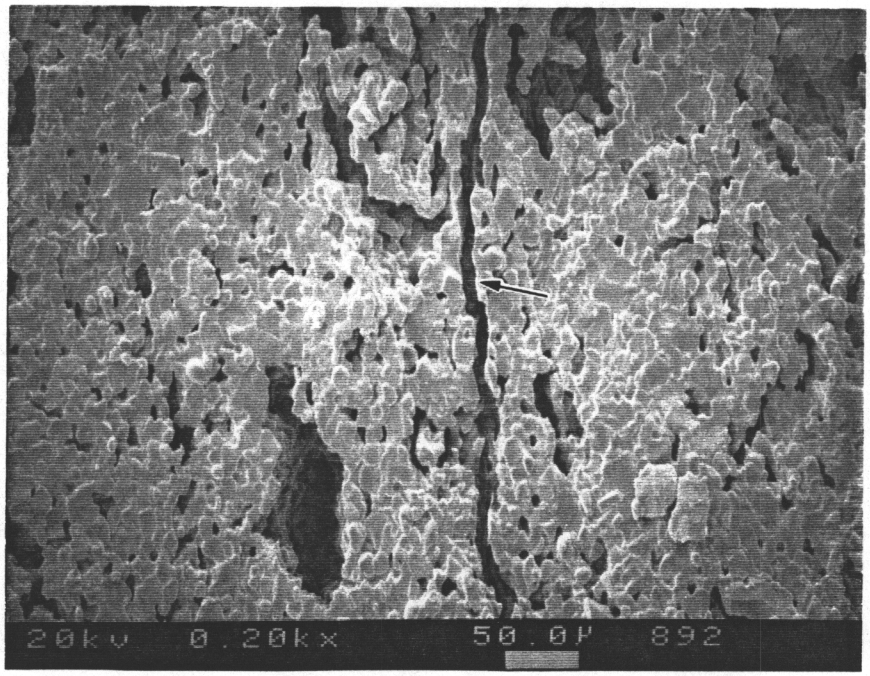

Figure 4.28 Fracture cracks due to thermal shock.

the extensibility for x=0.1 is nearly twice as that for x=0.3. That is to say, a higher capability of absorbing strain energy resulting from thermal shock can be achieved when x=0.1. This is due in part to the near-zero CTE, which is due to the grain size effect (Fig.4.11) that minimize the thermal stresses, and results in excellent thermal shock resistance.

The thermal stress resistance of the lightweight CMZP and ZrO_2 ceramics can be determined by substituting the porosity dependence of tensile strength and Young's moduli into eq.(2-5); for convenience, the resulting equations are expressed as a function of relative density:

$$x=0.0, \quad \Delta T = A * 10^{2.72-1.37(\rho/\rho s)} \tag{4-15}$$

$$x=0.1, \quad \Delta T = A * 10^{2.36-1.24(\rho/\rho s)} \tag{4-16}$$

$$x=0.2, \quad \Delta T = A * 10^{2.07-1.04(\rho/\rho s)} \tag{4-17}$$

$$x=0.3, \quad \Delta T = A * 10^{2.71-1.248(\rho/\rho s)} \tag{4-18}$$

$$\text{for } ZrO_2, \quad \Delta T = A * 10^{1.739-0.225(\rho/\rho s)} \tag{4-19}$$

where $A = \dfrac{k_p\,(1-\nu)}{0.31\, r_m\, h}$, and $k_p = k_s\,(1-p)^{(19)}$ with k_s being the thermal conductivity of the dense CMZP and ZrO_2 ceramics.

From the above equations, the thermal stress resistance of lightweight CMZP and ZrO_2 ceramics increases as porosity increases. Figure 4.29, obtained from the above equation using $(\rho/\rho_s)=0.55$ and $\nu=0.2$, illustrates the variation in

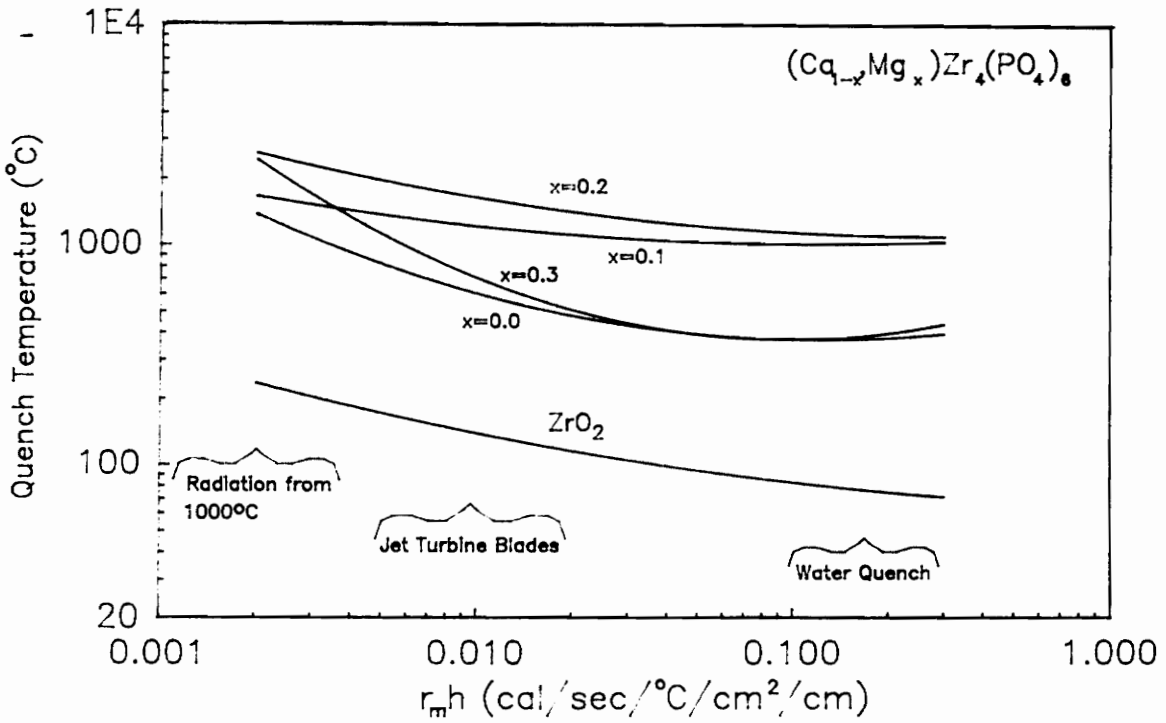

Figure 4.29 Thermal stress resistance of lightweight CMZP ceramics for different heat transfer conditions

quench temperature causing fracture under different conditions of heat transfer, assuming that failure occurs when the thermal stress reaches the tensile stress[23]. As shown, lightweight CMZP ceramics exhibit excellent thermal shock resistance as compared to ZrO_2.

The lightweight CMZP ceramics with compositions of x=0.0 and x=0.3 exhibit lower resistance than when x=0.1 and x=0.2 where $r_m h$ lies between 0.1 and 0.4. The lower calculated resistance may be due to higher TEA for x=0.0 and to lower thermal conductivity and higher Young's moduli for x=0.3.

4.7 Corrosion Resistance of Lightweight CMZP Ceramics

In Figure 4.30, the weight loss for the lightweight CMZP ceramics is within about 1 and 1.5 wt% in concentrated nitric and hydrochloric acid solutions, respectively. These small weight losses appear indicative of good chemical stability in acid environments.

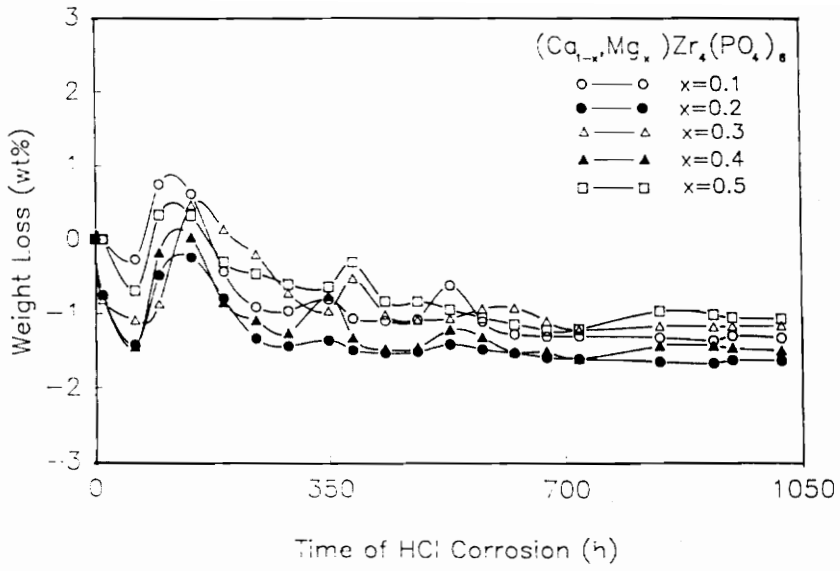

(a) in HCl

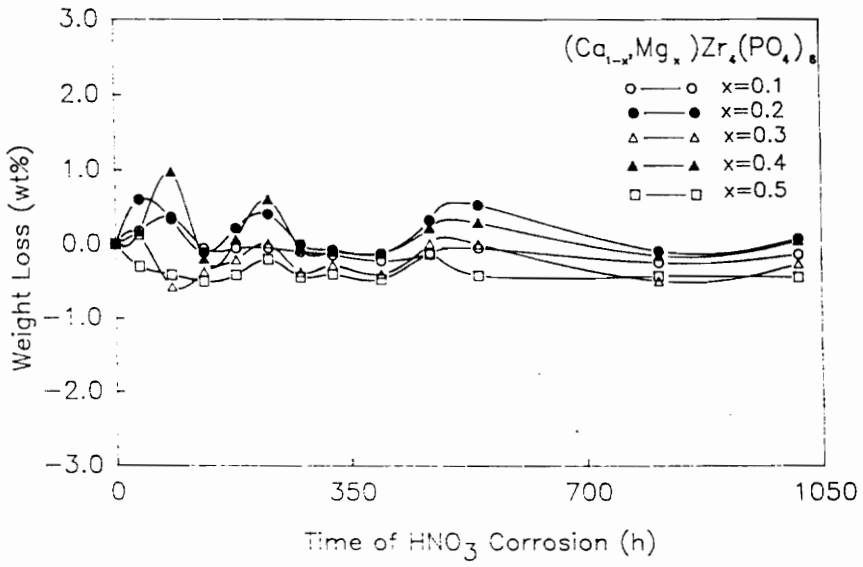

(b) in HNO_3

Figure 4.30 Weight loss versus corrosion time of lightweight CMZP ceramics in (a) HCl, (b)HNO_3 for over 1,000h.

CHAPTER 5.CONCLUSIONS

1. Lightweight CMZP ceramics were fabricated successfully using the polymer foam and polymer powder methods. The former technique produces large pores (250 μm) with a uniform open-pore structure, the latter yields small pores (30-80 μm) with a pore structure consisting of both open and closed pores.

2. Lightweight CMZP ceramics made by the polymer foam method exhibit higher gas permeability than those made by the polymer powder method.

3. The CTE of lightweight $(Ca_{1-x},Mg_x)Zr_4(PO_4)_6$ varies from negative to positive as $x>0.2$. Furthermore, the CTE is related to the microstructure. It decreases from positive to negative as the grain size increases, but is independent of the porosity content and processing technique.

4. Lightweight CMZP ceramics exhibit excellent thermal-shock resistance, due to the ultra-low CTE that minimizes the internal stresses. The thermal-shock resistance appears to increase with increasing porosity.

5. Dense CMZP ceramics exhibit thermal conductivity two to four times less than ZrO_2, a conventional thermal barrier material.

6. The tensile, compressive, and flexural strength of the lightweight CMZP ceramics generally exhibit higher values than those of the lightweight ZrO_2 for the same bulk density.

7. Lightweight CMZP ceramics are resistant to HCl and HNO_3 corrosion.

CHAPTER 6. REFERENCES

1. S.Y. Limate, D.K. Agrawal, and H.A. Mckinstry, "Synthesis and Thermal Expansion of $MZr_4P_6O_{24}$ (M= Mg,Ca,Sr,Ba)", J. Am. Ceram. Soc., **70**[10]c-232--c236(1987).

2. G.E. Lenain, H.A. Mckinstry, S.Y. Limate, and A. Woodword, "Low Thermal Expansion of Alkali--- Zirconium Phosphates", Mat. Res. Bull., **19** 1451-56(1984).

3. G.E. Lenain, H.A. Mckinstry, J. Alamo, and D.K. Agrawal, "Structural Model for Thermal Expansion in $MZr_2P_3O_{12}$ (M= Li,Na,K,Rb,Cs)", J. Mat. Sci., **22**[1]17-22(1987).

4. T. Kanazawa, Inorganic Phosphate Materials, Elservier Scientific Publisher, New York (1989).

5. F.F. Lange, and K.T. Miller, "Open-Cell, Low-Density Ceramics Fabricated from Reticulated Polymer Substrates", Adv. Ceram. Mat., **2**[4]827-31(1987).

6. D.J. Green, "Fabrication and Mechanical Properties of Lightweight Ceramics Produced by Sinter of Hollow Spheres", J. Am. Ceram. Soc., **68**[7]403-09(1988).

7. T. Fujiu, G.L. Messing, and W. Heubner, "Processing and Properties of Cellular Silica Synthesized by Foaming Sol-Gels", J. Am. Ceram. Soc., **73**[1]85-90(1990).

8. P.K.G. Wiggs, "The Relation Between Gas Permeability and Pore Structure of Solids", pp183-94 in Structure and Properties of Porous Materials edited by D.H. Everett and F.S. Stone, Butterworth Scientific Publisher, New York (1958).

9. H.Y.-P. Hong, " Crystal Structure and Crystal Chemistry in the System $Na_{1+x}Zr_2Si_xP_{3-x}O_{12}$", Mat. Res. Bull.,**11** 173-82(1976).

10. J. Alamo and R. Roy, "Crystal Chemistry of the $NaZr_2(PO_4)_3$, NZP or CTP, Structure Family", J. Mat. Sci., **21** 444-50(1986).

11. L.O. Hagman and P. Kierkegaard, "The Crystal Structure of $NaM^{IV}_2(PO_4)_3$, M^{IV} = Ge,Ti,Zr", Acta. Chem. Scand., **22** 1822-89(1986).
12. J.B. Goodenough, H.Y-P. Hong, and J.A. Kafalas, "Fast Na^+---Ion Transport in Skeleton Structures", Mat. Res. Bull., **11** 203-06(1976).

13. J.A. Kuszky and R.C. Brade, "Influence of Grain Size Effects of Thermal Expansion Anisotropy in $MgTi_2O_5$", J. Am. Ceram. Soc., **56**[8]420-23(1973).

14. R.W. Rice and R.C. Pohanka, "Grain-Sized Dependence of Spontaneous Cracking in Ceramics", J. Am. Ceram. Soc., **62**[11-12]559-63(1979).

15. J.J. Cleveland and R.C. Bradt, "Grain Size/Microcracking Relations for Pseudobrookite Oxides", J. Am. Ceram. Soc., **61**[11-12]478-81(1978).

16. W.D. Kingery and M.C. Mcquarrie, "Thermal Conductivity: I, Concepts of Measurement and Factors Affecting Thermal Conductivity of Ceramic Materials", J. Am. Ceram. Soc., **37**[2]67-72(1954).

17. A.L. Loeb, "Thermal Conductivity: VIII, A Theory of Thermal Conductivity of Porous Material", J. Am. Ceram. Soc., **37**[2]96-99(1954).

18. J. Francl and W.D. Kingery, " Thermal Conductivity: IX, Experimental Investigatation of Effect of Porosity on Thermal Conductivity", J. Am. Ceram. Soc., **37**[2]99-107(1954).

19. D.P.H. Hasselman, "Effect of Micro-cracking on Thermal Conductivity: Analysis and Experiment", pp417-31 in Thermal Conductivity edited by D,C. Larsen, Plenum Press, New York (1982)

20. H.J. Siebeneck, D.P.H. Hasselman, J.J. Cleveland, and R.C. Bradt, "Effect of Microcracking on the Thermal Diffusivity of Fe_2TiO_5", J. Am. Ceram. Soc., **59**[5-6]241-44(1976).

21. P.F. Becher, D. Lewis III, K.R. Carman, and A.C. Gonzales, "Thermal Shock Resistance of Ceramics: Size and Geometry Effects in Quench Tests", Am.

Ceram. Soc. Bull.,**59**[5]542-48(1980).

22. R.L. Coble and W.D. Kingery, "Effect of Porosity on Thermal Stress Fracture", J. Am. Ceram. Soc., **38**[1]33-37(1955).

23. W.D. Kingery, "Factors Affecting Thermal Stress Resistance of Ceramic Materials",J. Am. Ceram. Soc., **38**[1]3-14(1955).

24. D.P.H. Hasselman, "Unified Theory of Thermal Shock Fracture Initiation and Crack Propagation in Brittle Ceramics", J. Am. Ceram. Soc., **52**[11]600-04(1969).

25. D.P.H. Hasselman, "Elastic Energy at Fracture and Surface Energy as Design Critia for Thermal Shock", J. Am. Ceram. Soc., **46**[11]535-40(1963).

26. T.K. Gupta," Strength Degradation and Crack Propagation in Thermally Shocked Al_2O_3", J. Am. Ceram. Soc., **55**[5]249-53(1972).

27. R.W. Rice, "Effect of Inhomogeneous Porosity on Elastic Properties of Ceramic", J. Am. Ceram. Soc., **58**[9-10]458-59(1975).

28. R. Spriggs, "Expression for Effect of Porosity on Elastic Modulus of Polycrystalline Refractory Materials, Particularly Aluminum Oxide", J. Am. Ceram. Soc., **44**[5]628-29(1961).

29. B.D. Agarwal, G.A. Panizza, and L.J. Broutman, "Micromechanics Analysis of Porous Filled Ceramic Composites", J. Am. Ceram. Soc., **54**[12]620-24(1971).

30. M.F. Ashby, "The Mechanical Properties of Cellular Solids", Metal. Trans. A, **14A** 1755-69(1983).

31. L.F. Nielsen, "Elasticity and Damping of Porous Materials and Impregnated Materials", J. Am. Ceram. Soc., **67**[2]93-98(1984).

32. R.W. Rice, "Microstructure Dependence of Mechanical Behavior of

Ceramic", pp200-381 in Treatise on Material Science and Technology V11 edited by R.K. MacCrone, Academic press, New York (1977).
33. E. Ryshkewitch, "Compressive Strength of Porous Sintering Alumina and Zirconia" J. Am. Ceram. Soc., **36**[2]65-68(1953).

34. K.K. Schiller, "Porosity and Strength of Brittle Solid", pp35-49 in Mechanical Properties of Non-Metallic Brittle Materials edited by W.H. Walton, Wiley(Interscience), New York (1958).

35. P. Hrma and V. Satara, "Model for Strength of Brittle Porous Materials", J. Am. Ceram. Soc., **57**[2]71-73(1974).

36. R.E. Gannon, G.M. Harris, and T. Vasilos, "Effect of Porosity on Mechanical, Thermal, and Dielectric Properties of Fused Silica", Am. Ceram. Soc. Bull., **44**[5]460-62(1965).

37. F.P. Kundsen, "Dependence of Mechanical Strength of Brittle Polycrystalline Specimens on Porosity and Grain Size", J. Am. Ceram. Soc., **42**[8]376-87(1959).

38. R.B. Bird, Transport Phenomena, John Wiley and Sons Inc., New York (1960).

39. R.L. Coble and W.D. Kingery, "Effect of Porosity on Physical Properties of Sintered Alumina",J. Am. Ceram. Soc., **39**[11]377-85(1956).

40. S.M. Van Aken, "Thermal Expansion and Thermal Conductivity of $(Ca_{1-x},Mg_x)Zr_4(PO_4)_6$ where x=0.0-0.4", Master Thesis, Virginia Polytechnic Institute and State University, (1990).

41. D.K. Agrawal and R. Roy, "Composite Route to "Zero" expansion Ceramics", J. Mat. Sci., **20** 4617-23(1985).

42. I. Yamai and T. Oota,"Low-Thermal-Expansion Polycrystalline Zirconyl Phosphate Ceramic: Solid-Solution and Microcracking-Related Properties", J. Am. Ceram. Soc., **70**[8]585-90(1987).

43. W.R. Buessem; pp127-48 in Mechanical Properties of Engineering Ceramics, edited by W.W. Kriegel and H. PalmourIII, Interscience Publishers Inc. New York(1961).

44. W.R. Manning, O. Hunter, Jr., F.W. Calderwood, and D.W. Stacy, " Thermal Expansion of Nb_2O_5", J. Am. Ceram. Soc., **55**[7]342-47(1972).

45. K. Noguchi, M. Fujita, J. Masaki, and M. Mizushina, "Tensile Strength of Yttria-Stabilized Tetragonal Zirconia Polycrystals", J. Am. Ceram. Soc., **72**[7]1305-07(1989).

46. R.L. McCullough, "Generalized Combining Rules for Predicting Transport Properties of Composite Materials", Composites Science and Technology, **22**[1]3-21(1985).

VITA

The author was born on July 27, 1961 in Taiwan, Republic of China. He attended the Chung Yuan Christian University in Chung Li and received his B.S. in Chemical Engineering in June 1984. After graduation, he entered the graduate program in Materials Engineering at Virginia Polytechnic Institute and State University.